Chapter 9

Modeling Canopy Photosynthesis

Kouki Hikosaka*
Graduate School of Life Sciences, Tohoku University, Sendai 980-8578, Japan

CREST, JST, Tokyo, Japan

Tomo'omi Kumagai
Institute for Space-Earth Environmental, Nagoya University, Chikusa-ku, Nagoya 464-8601, Japan

and

Akihiko Ito
National Institute for Environmental Studies, Tsukuba, Ibaraki 305-8506, Japan

Summary 240
I. Introduction 240
II. Advances in Canopy Photosynthesis Models 241
III. Models of One-Dimensional Canopy Photosynthesis 242
A. Multi-layer Model 242
B. Big-Leaf Model 242
C. Sun–Shade Model 244
D. Comparison of Calculated Rates Between Canopy Photosynthesis Models 244
1. Multi-layer Model Under Direct–Diffuse Light (MDDM) 244
2. Multi-layer Model With Simple Light Extinction (MSM) 249
3. Big-Leaf Model 1 (BLM1) 249
4. Big-Leaf Model 2 (BLM2) 249
5. Sun–Shade Big-Leaf Model (SSM) 250
IV. Effect of Canopy Traits on Canopy Photosynthesis 251
V. Canopy Photosynthesis Models with Heat Exchange 254
VI. Validation 256
A. Plant Growth and Model Prediction 256
B. Eddy Covariance and Model Prediction 257
VII. Application of Canopy Photosynthesis Models to Larger Scales 260
VIII. Conclusion 264
Acknowledgments 264
References 264

*Author for correspondence, e-mail: hikosaka@m.tohoku.ac.jp

e-mail: tomoomikumagai@gmail.com

e-mail: itoh@nies.go.jp

K. Hikosaka, Ü. Niinemets, and N.P.R. Anten (eds.), *Canopy Photosynthesis: From Basics to Applications*, DOI 10.1007/978-94-017-7291-4_9

Summary

Canopy photosynthesis models (CPMs) calculate canopy photosynthetic rate as a sum of leaf photosynthetic rate. Here we focus on one-dimensional CPMs and show that simulated rates of canopy photosynthesis vary depending on whether multiple layers or a monolayer are considered and on whether direct and diffuse light sources are considered. We discuss how canopy photosynthetic rates vary depending on plant traits, which can differ within and among species; canopy photosynthetic rates are sensitive to leaf area index, light extinction coefficient, leaf photosynthetic capacity (photosynthetic nitrogen use efficiency), and nitrogen allocation between leaves. CPMs can predict exchange rates not only for carbon but also for water and energy. The predicted rates are consistent with observations. Finally, we describe how CPMs have been utilized for vegetation and global studies.

Keywords Atmosphere-ecosystem interaction • Big-leaf model • Canopy photosynthesis • Diffuse light • Direct light • Energy balance • Global environmental change • Leaf area index • Light extinction coefficient • Multi-layer model • Thermally produced turbulence effect • Uncertainty and model validation

I. Introduction

By definition, canopy photosynthesis is the sum of the photosynthetic rates of all leaves in the canopy. The complexity of canopy photosynthesis was first described by Boysen-Jensen (1932), who demonstrated that light dependence of canopy photosynthesis differs from that of leaves isolated from the canopy (see also Hirose 2005). It differs because leaves are exposed to different environmental conditions depending on their position in the canopy, and have different morphological and physiological traits depending on their environment and ontogeny, as has been discussed in previous Chaps. 1, 2, 3, 4, 5 (Goudriaan 2016; Gutschick 2016; Hikosaka et al. 2016; Niinemets 2016; Pons 2016). Current canopy photosynthesis models (CPMs) have incorporated these issues and photosynthetic performance of each leaf in the canopy, and permit the estimation of canopy gas exchange rate, such that predicted values are close to observations. Here we review the development of CPMs, focusing mainly on one-dimensional models and how they show the dependence of canopy photosynthetic rates on environmental variables and on plant or canopy traits. We also highlight how CPMs play important roles in terrestrial carbon cycle models and dynamic

Abbreviations (See Table 9.1 for Model Parameters in Box 9.2): A – Photosynthetic rate; a_l – Albedo; a_V – Slope of V_{cmax}-N relationship; BLM – Big-leaf model; C_i – Intercellular CO_2 partial pressure; c_p – Specific heat of air; CPM – Canopy photosynthesis model; d – Zero-plane displacement; E – Evapotranspiration rate; e – Vapor pressure; G – Heat flux into thermal storage; g – Conductance; GPP – Gross primary production; H – Sensible heat flux; I_c – Absorbed light per unit leaf area; IBP – International Biological Programme; k – Extinction coefficient; L – Cumulative leaf area index; LUE – Light use efficiency; l – Monin-Obukhov length; LAI – Leaf area index; m_a – and m_e Molecular weights of air and water; MDDM – Multilayer model under direct-diffuse light; MSM – Multilayer model with simple light extinction; N – Nitrogen content; NDVI – Normalized difference vegetation index; NEE – Net ecosystem CO_2 exchange; NPP – Net primary production; P – Atmospheric pressure; PFD – Photosynthetially active photon flux density; R – Radiation; RE – Ecosystem respiration; SS – Sunshade big-leaf model; T – Temperature; u – Wind velocity; V_{cmax} – Maximum rate of carboxylation; z – Height; z_{0H} – and z_{0M} Roughness lengths for heat and momentum; γ – Psychrometric constant in Eq. 9.6; κ – von Karman constant; ρ – Density of air; λ – Heat of vaporization; θ – Convexity of photosynthetic curves; χ_H – and χ_M Dimensionless temperature and velocity profiles; X_{dif} – X for diffuse light; X_{dir} – X for direct light; X_{sca} – X for scattering light; X_{sh} – X for shade leaf; X_{sca} – X for sunlit leaf; n – Value of X at the top of the canopy; X_t – Value of X per ground area

vegetation models and how they have contributed to the understanding and projection of global carbon balance.

II. Advances in Canopy Photosynthesis Models

The first CPM was developed by Monsi and Saeki (1953). They assessed canopy structure using a stratified clipping method and determined vertical profiles of leaf and light distribution. They found that light distribution can be described by an exponential function like the Beer–Lambert law, and the slope (extinction coefficient, k) can differ among stands depending mainly on leaf angle. A rectangular hyperbola was used to express the light-response curve of photosynthesis, and the canopy photosynthetic rate was calculated as the sum of leaf photosynthetic rates. This model successfully included the essential parts of canopy photosynthesis in a mathematical manner.

Models of light distribution were further developed, for instance, by separate distributions of direct and diffuse light, solar angle, and leaf angle distributions (de Wit 1965; Gourdriaan 1977, see Chap. 1, 2016).

Leaf canopies are characterized by vertical gradients in leaf photosynthetic properties (Saeki 1959; see Chap. 4, Niinemets 2016). However, until the early 1980s, such gradients were ignored in CPMs (i.e., all leaves in the canopy were assumed to have the same characteristics), owing mainly to limitation in computation abilities. To incorporate such variation, Hirose and Werger (1987a) introduced a two-step process first determining the relationships between the parameters of the light-response curve of photosynthesis (maximum rate, respiration rate, initial slope, and convexity of the curve), and leaf nitrogen content and then calculating the leaf N distribution in the canopy.

For leaf photosynthesis, earlier models incorporated only light as an environmental variable. Farquhar et al. (1980) developed a biochemical model of leaf photosynthesis in which CO_2 assimilation rates are expressed as the function of light, CO_2 concentration, and temperature. Ball et al. (1987) proposed an empirical model of stomatal conductance as a function of air humidity, CO_2 concentration, and photosynthetic rate. Combining these models permits the estimation of gas exchange rates under fluctuating environmental conditions (Harley and Tenhunen 1991; Harley et al. 1992; Baldocchi 1994; Harley and Baldocchi 1995; see Chap. 3, Hikosaka et al. 2016).

During the 1990s, several CPMs that incorporated light distribution, leaf property gradient, and leaf physiology were developed (e.g., MAESTRO: Wang and Jarvis 1990). Some of them incorporated heat fluxes (e.g., CANOAK: Baldocchi and Harley 1995). The predicted gas exchange rate was strongly correlated with the rate measured by the eddy covariance method (Baldocchi and Harley 1995). Nowadays, we can accurately predict canopy gas exchange if canopy characteristics and environmental variables are given.

Alternative efforts have been made to describe canopy photosynthesis using simpler models that minimize calculation time and the need for parameterization. The simplest model expresses canopy productivity as the product of light use efficiency (or radiation use efficiency), interception efficiency and solar radiation (Monteith 1972).

Farquhar (1989) showed that an equation describing whole-leaf photosynthesis has the same form as one for individual chloroplasts across a leaf, provided the distribution of chloroplast photosynthetic capacity is in proportion to the profile of absorbed irradiance and that the shape of the response to irradiance is identical in all layers. This led to a new generation of big-leaf models (BLMs; see Sect. III.B) for canopy photosynthesis. BLMs treat the canopy as a layer of one big leaf. Some studies have simply applied a leaf photosynthesis model to calculation of canopy photosynthetic rates (e.g., Lloyd et al. 1995). However, most BLMs did not separate direct from diffuse light in the canopy. de Pury and Farquhar (1997) developed a single layered model that separately accounts for beam and diffuse lights, and is as accurate as, but simpler than, multi-layer models. Several ecosystem models use the

model of de Pury and Farquhar (1997) for calculating canopy photosynthesis.

CPMs have been incorporated into terrestrial ecosystem models (Table 9.2), which play important roles for understanding the present processes and in making future projections under global environmental change. For example, terrestrial carbon cycle models, such as the Vegetation Integrated SImulator for Trace gases (VISIT: Ito et al. 2005) and the Biosphere Model integrating Eco-physiology and Mechanistic approaches using Satellite data (BEAMS: Sasai et al. 2005), use canopy models to estimate ecosystem carbon uptake from the atmosphere. Similarly, several dynamic vegetation models, such as the Lund–Potsdam–Jena (LPJ: Sitch et al. 2003) and the Organized Carbon and Hydrology in Dynamic Ecosystems (ORCHIDEE: Krinner et al. 2005) models, include canopy models but in a relatively simple manner. Because these vegetation canopy models are used to estimate carbon and water budgets of ecosystems, their uncertainty eventually influences estimation of future ecosystem responses and feedback to global change.

CPMs have also been incorporated into crop models (van Ittersum et al. 2003). Simple models used relationships between radiation and crop growth based on the light use efficiency (e.g., LINTUL: Spitters and Schapendonk 1990). Some models are a mechanistic models that consider CO_2 assimilation and respiration as a function of environmental conditions (e.g., SUCROS: Goudriaan and van Laar 1994). Recent models consider the spatiotemporal dynamics of growth and development of plants, where complex three-dimensional structures of individual plants are combined with physiological mechanisms (functional–structural plant models, FSPM; see Chap. 8, Evers 2016).

III. Models of One-Dimensional Canopy Photosynthesis

A. Multi-layer Model

In most multi-layer models, the canopy comprises many horizontal layers. Light from top to bottom of the canopy is modeled, and absorbed light by leaves in each layer is calculated as described in Chap. 1 (Goudriaan 2016). In earlier models, light availability was assumed to be identical among leaves within each layer, whereas more advanced models consider sunlit and shaded leaves separately (Fig. 9.1). Sunlit leaves receive both direct and diffuse light, whereas shaded leaves receive only diffuse light. In general, leaf angle is assumed to be identical, or mean values are used, but some models consider leaves with different angles separately (e.g., Anten and Hirose 2003). In earlier models, leaf photosynthetic traits were assumed to be identical among leaves, whereas recent models incorporate vertical distributions of photosynthetic capacity or nitrogen content as an exponential or linear functions of canopy depth (normally expressed as cumulative leaf area index from the top of the canopy). In some models, differences in leaf traits among individuals or species are taken into account (Anten and Werger 1996; Hikosaka et al. 1999; Anten and Hirose 2003; See Chap. 14, Anten and Bastiaans 2016). Canopy photosynthetic rate is calculated as the sum of photosynthetic rates of leaves (Fig. 9.1).

B. Big-Leaf Model

BLMs treat the canopy as if it were a single-layer leaf. There are several types of BLMs. The simplest one applies a leaf photosynthesis model to the canopy (Amthor 1994; Lloyd et al. 1995), with assimilation rates expressed per unit ground area instead of per unit leaf area. This model is used when data of environmental dependence of stand CO_2 exchange are available for parameter calibration, by which model estimates are adjusted to observations.

A slightly more elaborate BLM derives canopy photosynthesis A_t as an integral of photosynthesis from top leaves with some assumptions:

$$A_t = A_o \frac{1 - \exp(-kL)}{k} \qquad (9.1)$$

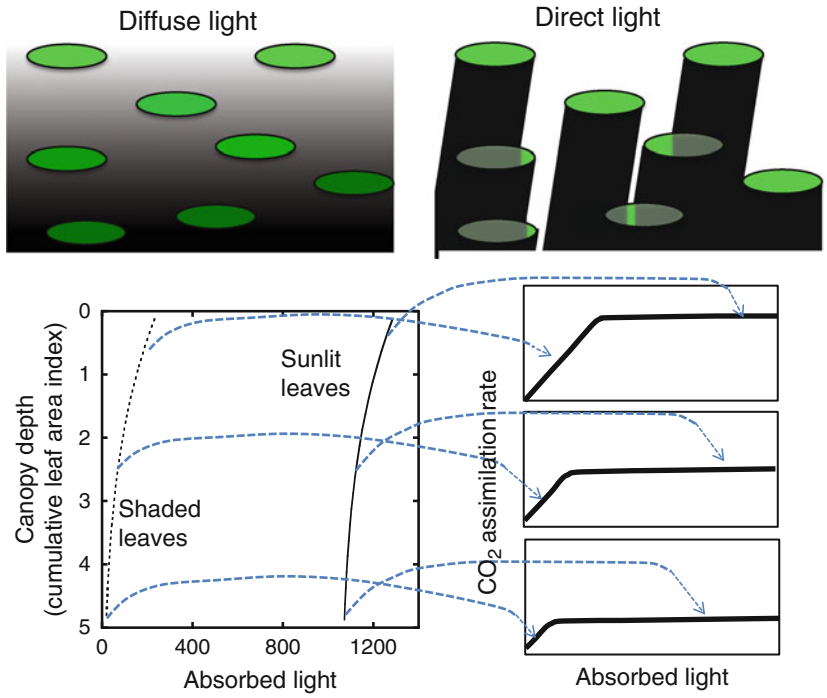

Fig. 9.1. Principle of the canopy photosynthesis model. Diffuse light diminishes in intensity with canopy depth, whereas direct light diminishes in area with canopy depth. Sunlit leaves receive direct and diffuse light whereas shaded leaves receive only diffuse light. CO_2 assimilation rates are calculated for sunlit and shaded leaves in each layer

where A_o denotes the photosynthetic rate of the top leaf in the canopy. The term $1 - \exp(-kL)$ is the fraction of the incident light that is absorbed by the canopy. This equation assumes the photosynthetic capacity (light-saturated rate of photosynthesis, $A_{\max}$) of a leaf to be proportional to the relative light availability that it receives; for example, if a leaf receives only 50 % of the light, its $A_{\max}$ is also 50 % of $A_{\max}$ of top leaves. It further assumes other environmental factors (such as humidity and temperature) to be identical among layers (See Box 9.1 for how this equation is derived). The environmental response of A_o can be simulated by the biochemical model of the photosynthesis as shown in Chap. 3 (Hikosaka et al. 2016).

Box 9.1 Derivation of Big-Leaf Model

Here we apply a rectangular hyperbola for gross leaf photosynthesis A.

$$A = \frac{A_{\max}\phi I_c}{A_{\max} + \phi I_c} \qquad \text{(B9.1.1)}$$

where $A_{\max}$, ϕ, I_c are light-saturated rate, the initial slope and the absorbed light by the leaf, respectively.

Light extinction is described by Beer's law.

$$I = I_o \exp(-kL) = I_o q \qquad \text{(B9.1.2)}$$

(continued)

Box 9.1 (continued)

where I_o, k, L and q is the light intensity above the canopy, light extinction coefficient, cumulative leaf area index from the top, and relative light intensity. Ignoring light scattering by leaves, I_c is derived from the differentiate of I.

$$I_c = I_o k \exp(-kL) \qquad \text{(B9.1.3)}$$

Here we assume that A_{max} of a leaf is proportional to q.

$$A_{max} = A_{omax} q \qquad \text{(B9.1.4)}$$

where A_{omax} is A_{max} of the top leaf. Canopy photosynthesis A_t is give as the integral of leaf photosynthesis.

$$A_t = \int_0^{L_{max}} A \; dL \qquad \text{(B9.1.5)}$$

Substituting Eqs. B9.2.2 and B9.2.5 to Eq. B9.2.6, A_t is derived as follows

$$\begin{aligned} A_t &= \int_0^{L_{max}} \frac{A_{omax} q \phi I_c}{A_{omax} q + \phi I_c} dL \\ &= \int_0^{L_{max}} \frac{A_{omax} \exp(-kL) \phi k I_o \exp(-kL)}{A_{omax} \exp(-kL) + \phi k I_o \exp(-kL)} dL \\ &= \frac{A_{omax} \phi I_{oc}}{A_{omax} + \phi I_{oc}} \int_0^{L_{max}} \exp(-kL) dL \\ &= A_o \frac{1 - \exp(-kL)}{k} \end{aligned} \qquad \text{(B9.1.6)}$$

where A_o is A of the top leaf.

C. Sun–Shade Model

One of the shortcomings of BLMs is that they consider only average light level at each layer and ignore direct and diffuse light, which have different canopy-transfer and photosynthetic properties. Given that the light-response curve of photosynthesis is concave, an increase in light intensity increases photosynthesis in low light but not in high light. Thus, a difference in frequency of light intensity affects photosynthetic rates even when average light intensities are similar. de Pury and Farquhar (1997) developed an adjustment to the above-mentioned BLM that considered the difference between direct (beam) and diffuse light and scattering within the canopy. The model divides the canopy into two components: sunlit and shaded leaves. Shaded leaves receive only diffuse light, whereas sunlit leaves receive both direct and diffuse light. Canopy photosynthesis is calculated as the sum of photosynthesis of sunlit and shade leaves.

D. Comparison of Calculated Rates Between Canopy Photosynthesis Models

Here we use five CPMs.

1. Multi-layer Model Under Direct–Diffuse Light (MDDM)

In this model, solar geometry and photosynthetically active photon flux density (PFD) above the canopy were modeled as described in Box 1.1 of Chap. 1 (Goudriaan 2016) (equations are shown in Box 9.2; Eqs. B9.2.1, B9.2.2, B9.2.3, B9.2.4 and B9.2.5). The canopy comprised multiple layers (in this example, 20 layers) in which leaves were randomly distributed. Leaves received direct PFD $I_{c,dir}$, diffuse PFD $I_{c,dif}$, and scattered direct PFD $I_{c,sca}$. An example is shown in Fig. 9.2. $I_{c,dir}$ was constant across the layers (Eq. B9.2.7), but the fraction of leaves receiving direct PFD decreased with canopy depth (Eq. B9.2.6). $I_{c,dif}$ decreased with canopy depth (Eq. B9.2.8). $I_{c,sca}$ was calculated as the difference between light interception by black (no scattering) and actual leaves (Eq. B9.2.9). Sunlit leaves received $I_{c,dir}$, $I_{c,dif}$, and $I_{c,sca}$ whereas shade leaves received $I_{c,dif}$, and $I_{c,sca}$ (Eqs. B9.2.10 and B9.2.11). The light extinction coefficient for direct light was calculated as a function of leaf angle and solar angle (Anten 1997; Kamiyama et al. 2010; Eqs. B9.2.12, B9.2.13 and B9.2.14). The light extinction coefficient for diffuse light k_{dif} was assumed to depend on the leaf inclination angle: 0.5, 0.7, and 0.9 when this angle was 75°, 45°, and 15°, respectively.

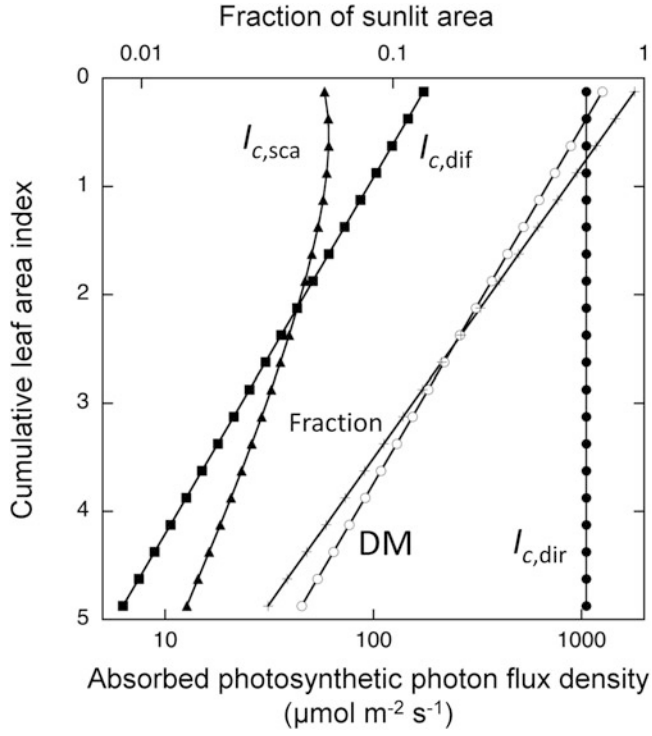

Fig. 9.2. An example of a vertical profile of photosynthetically active photon flux density (PFD). Assumptions include 1200 on a cloudless vernal equinox day at the equator in and leaf angle of 45°. A canopy with leaf area index of 5 was divided into 20 layers and absorbed PFD was calculated. $I_{c,\mathrm{dir}}$ is absorbed PFD of direct light per unit sunlit leaf area. $I_{c,\mathrm{dif}}$ and $I_{c,\mathrm{sca}}$ denote absorbed PFD of diffuse and scattered direct light per unit total leaf area in each layer, respectively. MSM (diffuse-light model) denotes the absorbed PFD per leaf area when all the light above the canopy is assumed to be diffuse light (see text). Fraction is the fraction of sunlit area in each layer

For simplicity, leaf angle was assumed to be constant within the canopy. PFD absorption was calculated assuming that it was identical among sunlit leaves and among shade leaves within each layer (Eqns B9.2.6′, B9.2.8′, and B9.2.9′).

Box 9.2 Equations Used in the Models

See Table 9.1 for abbreviations and units.

1. Solar geometry (see Chap. 1 Goudriaan 2016)

$$\sin\delta = -\frac{23.44\pi}{180}\cos\frac{2\pi\left(t_{\mathrm{day}}+10\right)}{365.24} \qquad \text{(B9.2.1)}$$

$$\sin\beta = \sin\lambda\sin\delta + \cos\lambda\cos\delta\cos\frac{2\pi(t_h-12)}{24} \qquad \text{(B9.2.2)}$$

2. Multi-layer model under direct-diffuse light (MDDM)

2.1 PFD above the canopy

$$I_{\mathrm{dir}} = a^m I_e \sin\beta \qquad \text{(B9.2.3)}$$

$$m = \frac{P}{P_o\sin\beta} \qquad \text{(B9.2.4)}$$

$$I_{\mathrm{dif}} = f_a(1-a^m)I_e\sin\beta \qquad \text{(B9.2.5)}$$

2.2 Light absorption at depth L (see Chap. 1 Goudriaan 2016)

(continued)

Box 9.2 (continued)

$$f_{su} = \exp\left(-k'_{dir}L\right) \quad \text{(B9.2.6)}$$

$$I_{c,dir} = (1-\sigma)k'_{dir}I_{dir} \quad \text{(B9.2.7)}$$

$$I_{c,dif} = (1-\rho_{dif})k_{dif}I_{dif,0}\exp(-k_{dif}L) \quad \text{(B9.2.8)}$$

$$I_{c,sca} = I_{dir}(1-\rho_{dir})k_{dir}\exp(-k_{dir}L) - I_{dir}(1-\sigma)k'_{dir}\exp\left(-k'_{dir}L\right) \quad \text{(B9.2.9)}$$

$$I_{c,su} = I_{c,dir} + I_{c,dif} + I_{c,sca} \quad \text{(B9.2.10)}$$

$$I_{c,sh} = I_{c,dif} + I_{c,sca} \quad \text{(B9.2.11)}$$

$$k_{dir} = \frac{O_{av}}{\sin\beta} \quad \text{(B9.2.12)}$$

$$O_{av} = \sin\beta\cos\alpha \quad \beta > \alpha \quad \text{(B9.2.13a)}$$

$$O_{av} = \frac{2}{\pi}\left(\sin\beta\ \cos\alpha \arcsin\frac{\tan\beta}{\tan\alpha} + \sqrt{\sin^2\alpha - \sin^2\beta}\right) \quad \alpha > \beta \quad \text{(B9.2.13b)}$$

$$k_{dir} = k'_{dir}\sqrt{1-\sigma} \quad \text{(B9.2.14a)}$$

$$k_{dif} = k'_{dif}\sqrt{1-\sigma} \quad \text{(B9.2.14b)}$$

2.3 Nitrogen content at depth L

$$N_l = \frac{k_b N_t \exp(-k_b L)}{1-\exp(-k_b L_t)} + N_b \quad \text{(B9.2.15)}$$

2.4 Light absorption and nitrogen content per unit leaf area in a layer between Ln+1 and Ln

$$f_{su} = \frac{\exp\left(-k'_{dir}L_n\right) - \exp\left(-k'_{dir}L_{n+1}\right)}{k'_{dir}(L_{n+1}-L_n)} \quad \text{(B9.2.6′)}$$

$$I_{c,dif} = (1-\rho_{dif})I_{dif,0}\frac{\exp(-k_{dif}L_n) - \exp(-k_{dif}L_{n+1})}{L_{n+1}-L_n} \quad \text{(B9.2.8′)}$$

$$I_{c,sca} = I_{dir}\frac{(1-\rho_{dir})[\exp(-k_{dir}L_n) - \exp(-k_{dir}L_{n+1})] - (1-\sigma)\left[\exp\left(-k'_{dir}L_n\right) - \exp\left(-k'_{dir}L_{n+1}\right)\right]}{L_{n+1}-L_n} \quad \text{(B9.2.9′)}$$

$$N_l = (N_o - N_b)\frac{\exp(-k_b L_n) - \exp(-k_b L_{n+1})}{k_b(L_{n+1}-L_n)} + N_b \quad \text{(B9.2.15′)}$$

where $N_o = \frac{k_b N_t}{1-\exp(-k_b L_t)} + N_b$.

2.5 Gas exchange (see Chap. 3)

$$\theta_{cj}A^2 - A\left(A_c + A_j\right) + A_c A_j = 0 \quad \text{(B9.2.16)}$$

$$A_c = \frac{V_{cmax}\left(C_i - \Gamma^*\right)}{C_i + K_c(1+O/K_o)} - R_d \quad \text{(B9.2.17)}$$

$$A_j = \frac{J\left(C_i - \Gamma^*\right)}{4C_i + 8\Gamma^*} - R_d \quad \text{(B9.2.18)}$$

$$J = \frac{\phi_j I_c + J_{max} - \sqrt{\left(\phi_j I_c + J_{max}\right)^2 - 4\phi_j I_c J_{max}\theta_j}}{2\theta_j} \quad \text{(B9.2.19)}$$

$$V_{cmax} = V_{cmax25}\exp\left[\frac{E_{aV}(T_k - 298)}{298\boldsymbol{R}T_k}\right] \quad \text{(B9.2.20)}$$

$$R_d = R_{d25}\exp\left[\frac{E_{aR}(T_k - 298)}{298\boldsymbol{R}T_k}\right] \quad \text{(B9.2.21)}$$

$$J_{max25} = \frac{J_{max25}\exp\left[\frac{E_{aJ}(T_k-298)}{298\boldsymbol{R}T_k}\right]\left[1+\exp\left(\frac{298\Delta S - H_d}{298\boldsymbol{R}}\right)\right]}{1+\exp\left(\frac{T_k\Delta S - H_d}{\boldsymbol{R}T_k}\right)} \quad \text{(B9.2.22)}$$

$$V_{cmax25} = a_V(N_l - N_b) \quad \text{(B9.2.23)}$$

$$J_{max25} = a_J V_{cmax25} \quad \text{(B9.2.24)}$$

$$R_{25} = a_R V_{cmax25} \quad \text{(B9.2.25)}$$

$$A_t = \sum A \quad \text{(B9.2.26)}$$

(continued)

Box 9.2 (continued)

3. Multi-layer model with simple light extinction (MSM)
   3.1 PFD above the canopy

$$I_{\mathrm{dir}} = 0 \qquad \text{(B9.2.3}')$$

$$I_{\mathrm{dif}} = f_a(1-a^m)I_e \sin\beta + a^m I_e \sin\beta \qquad \text{(B9.2.5}')$$

Other equations are same as those in MDDM

4. Big-leaf model 2 (BLM2; de Pury and Farquhar 1997 with some modifications)
   PFD above the canopy is modeled as in MDDM
   4.1 Light absorption by the canopy

$$I_t = \int_0^{L_t} I_c dL = I_{\mathrm{dir}}(1-\rho_{\mathrm{dir}}) \{1-\exp(-k_{\mathrm{dir}}L_t)\} + I_{\mathrm{dif}}(1-\rho_{\mathrm{dif}}) \{1-\exp(-k_{\mathrm{dif}}L_t)\} \qquad \text{(B9.2.27)}$$

   4.2 Canopy gas exchange

$$\theta_{cj}A_t^2 - A_t(A_{ct}+A_{jt}) + A_{ct}A_{jt} = 0 \qquad \text{(B9.2.16}')$$

$$A_{ct} = \frac{V_{\mathrm{cmax}t}(C_i-\Gamma^*)}{C_i + K_c(1+O/K_o)} - R_{dt} \qquad \text{(B9.2.17}')$$

$$A_{jt} = \frac{J_t(C_i-\Gamma^*)}{4C_i+8\Gamma^*} - R_{dt} \qquad \text{(B9.2.18}')$$

$$J_t = \frac{\phi_j I_t + J_{\mathrm{max}t} - \sqrt{(\phi_j I_t + J_{\mathrm{max}t})^2 - 4\phi_j I_t J_{\mathrm{max}t}\theta_j}}{2\theta_j} \qquad \text{(B9.2.19}')$$

$$V_{\mathrm{cmax}t25} = a_V(N_t - L_t N_b) \qquad \text{(B9.2.23}')$$

$$J_{\mathrm{max}t25} = a_J V_{\mathrm{cmax}t25} \qquad \text{(B9.2.24}')$$

$$R_{dt25} = a_R V_{\mathrm{cmax}t25} \qquad \text{(B9.2.25}')$$

5. Sun–shade BLM (SSM, de Pury and Farquhar 1997 with some modifications)
   PFD above the canopy is modeled as in MDDM
   5.1 LAI of sunlit leaves

$$L_{\mathrm{su}} = \int_0^{L_t} f_{\mathrm{su}} dL = \frac{1-\exp(-k'_{\mathrm{dir}}L_t)}{k'_{\mathrm{dir}}} \qquad \text{(B9.2.28)}$$

Light absorption by the canopy is defined by B9.2.27.

   5.2 Light absorption of sunlit leaves

$$I_{t,\mathrm{su}} = \int_0^{L_t} I_{c,\mathrm{su}} f_{\mathrm{su}} dL = \int_0^{L_t} I_{c,\mathrm{dir}} f_{\mathrm{su}} dL + \int_0^{L_t} I_{c,\mathrm{dif}} f_{\mathrm{su}} dL + \int_0^{L_t} I_{c,\mathrm{sca}} f_{\mathrm{su}} dL \qquad \text{(B9.2.29)}$$

$$\int_0^{L_t} I_{c,\mathrm{dir}} f_{\mathrm{su}} dL = I_{\mathrm{dir}}(1-\sigma)\left[1-\exp\left(-k'_{\mathrm{dir}}L_t\right)\right] \qquad \text{(B9.2.29a)}$$

$$\int_0^{L_t} I_{c,\mathrm{dif}} f_{\mathrm{su}} dL = I_{\mathrm{dif}}(1-\rho_{\mathrm{dif}}) k_{\mathrm{dif}} \frac{1-\exp\left[-\exp\left(-k_{\mathrm{dif}}L_t - k'_{\mathrm{dir}}L_t\right)\right]}{k_{\mathrm{dif}}+k'_{\mathrm{dir}}} \qquad \text{(B9.2.29b)}$$

$$\int_0^{L_t} I_{c,\mathrm{sca}} f_{\mathrm{su}} dL = I_{\mathrm{dir}}(1-\rho_{\mathrm{dir}}) k_{\mathrm{dir}} \frac{1-\exp\left[-\exp\left(-k_{\mathrm{dir}}L_t - k'_{\mathrm{dir}}L_t\right)\right]}{k_{\mathrm{dir}}+k'_{\mathrm{dir}}} - I_{\mathrm{dir}}(1-\sigma)\frac{1-\exp\left(-2k'_{\mathrm{dir}}L_t\right)}{2} \qquad \text{(B9.2.29c)}$$

   5.3 Light absorption of shaded leaves

$$I_{t,\mathrm{sh}} = I_t - I_{t,\mathrm{su}} \qquad \text{(B9.2.30)}$$

(continued)

Box 9.2 (continued)

5.4 Total canopy photosynthetic capacity is calculated by B9.2.23′ Photosynthetic capacity of sunlit leaves

$$V_{cmaxf25,su} = \int_0^{L_t} V_{cmaxf25} f_{su} dL = a_V (N_o - N_b) \frac{1 - \exp\left(-k_b L_t - k'_{dir} L_t\right)}{k_b + k'_{dir}} \quad \text{(B9.2.31)}$$

5.5 Photosynthetic capacity of shaded leaves

$$V_{cmaxt,sh} = V_{cmaxt} - V_{cmaxt,su} \quad \text{(B9.2.32)}$$

5.6 Canopy photosynthesis

$$A_t = A_{t,su} + A_{t,sh} \quad \text{(B9.2.33)}$$

where $A_{t,su}$ and $A_{t,sh}$ are calculated using $V_{cmaxt,su}$ and $V_{cmaxt,sh}$, respectively, as A_t in BLM2.

Table 9.1. Abbreviations, units, and values used in the models

Symbol	Definition	Unit	Value
a	atmospheric transmission coefficient of PFD	–	0.72
A	Assimilation rate	μmol m^{-2} s^{-1}	–
A_c	RuBP-saturated A	μmol m^{-2} s^{-1}	–
Aj	RuBP-limited A	μmol m^{-2} s^{-1}	–
a_J	Ratio of J_{max25} to V_{cmax25}	–	2.1
a_R	Ratio of R_{d25} to V_{cmax25}	–	0.0089
a_V	Ratio of V_{cmax25} to photosynthetic nitrogen	s^{-1}	1.16×10^{-3}
C_i	Intercellular CO_2 partial pressure	Pa	25
E_{aJ}	Activation energy of J_{max}	J mol^{-1}	37,000
E_{aV}	Activation energy of V_{cmax}	J mol^{-1}	64,800
E_{aR}	Activation energy of R_d	J mol^{-1}	66,400
f_a	Forward scattering coefficient of PFD in atmosphere	–	0.426
f_{su}	Fraction of sunlit area	–	–
H_d	Deactivation energy	J mol^{-1}	220,000
LAI	Leaf area index	m^2 m^{-2}	–
I_c	Absorbed PFD	μmol m^{-2} s^{-1}	–
I_e	extra-terrestrial PFD	μmol m^{-2} s^{-1}	2413
J_{max}	Maximal rate of electron transport	μmol m^{-2} s^{-1}	–
k	Light extinction coefficient		
k'	Light extinction coefficient for 'black' leaves		
k_b	Nitrogen distribution coefficient		
K_c	Michaelis constant for CO_2	Pa	29.16 (at 21 °C)
K_o	Michaelis constant for O_2	kPa	20.35 (at 21 °C)
L	Cumulative leaf area index	m^2 m^{-2}	–
m	Optical air mass	–	–
N_b	Leaf structural nitrogen content	mmol m^{-2}	–
N_l	Leaf nitrogen content	mmol m^{-2}	–
O	O_2 partial pressure	kPa	20.5
O_{av}	Average projection of leaves in the direction of direct PFD	–	–
P	Air pressure	kPa	98.7
PFD	Photosynthetically active photon flux density	μmol m^{-2} s^{-1}	–
P_o	Air pressure at sea level	kPa	101.3

(continued)

Table 9.1. (continued)

Symbol	Definition	Unit	Value
R_d	Day respiration rate	μmol m^{-2} s^{-1}	–
$\boldsymbol{R}$	Gas constant	J mol^{-1} K^{-1}	8.314
t_{day}	Day of year	day	264
t_h	Time of day	hour	–
T_k	Leaf temperature	K	21 °C
V_{cmax}	Maximal rate of carboxylation	μmol m^{-2} s^{-1}	–
α	Leaf inclination angle	radians	–
β	Solar elevation angle	radians	–
δ	Solar declination angle	radians	–
ΔS	Entropy term for J_{max}	J mol^{-1} K^{-1}	710
ϕ_j	Initial slope of light-response curve of electron transport rate	mol mol^{-1}	0.425
Γ*	CO_2 compensation point in the absence of day respiration	Pa	3.0 (at 21 °C)
ρ_{dif}	Reflection coefficient for diffuse light	–	0.036
ρ_{dir}	Reflection coefficient for direct light	–	0.027
λ	Latitude	radians	0
θ_{cj}	Curvature factor for A_c–A_j transition	–	0.99
θ_j	Curvature factor for light-response of electron transport	–	0.7
σ	Leaf scattering coefficient	–	0.15
X_0	X of top leaves		
X_{25}	X at 25 °C		
X_{dif}	X of diffuse light		
X_{dir}	X of direct light		
X_{sca}	X of scattered light		
X_{sh}	X in shaded leaves		
X_{su}	X in sunlit leaves		
X_t	Amount of X in the canopy per unit ground area		

2. Multi-layer Model With Simple Light Extinction (MSM)

In this model we estimated the effect of not separating direct and diffuse light on canopy photosynthesis. To this end, PFD above and within the canopy was assumed to be diffuse light (without direct light). Total PFD above the canopy was the same as that in the MDDM. Other variables were same as for MDDM.

3. Big-Leaf Model 1 (BLM1)

In this model, we calculated photosynthesis of top leaves A_0 using PFD above the canopy ($I_{c,dir} + I_{c,dir,o}$) and nitrogen content of top leaves (N_o; see Eq. B9.2.15). A_t was derived by Eq. 9.1.

4. Big-Leaf Model 2 (BLM2)

The BLM2 is a type of modified BLM described by de Pury and Farquhar (1997). In this model, the variation in nitrogen content in the canopy is taken into account. PFD absorbed by the canopy on a ground-area basis was calculated by Eq. B9.2.27. Canopy photosynthetic capacity V_{cmaxt} was calculated from total canopy nitrogen content N_t (B9.2.23′) and other rates were simply obtained as that for leaves (Eqs. B9.2.24′ and B9.2.25′). A_t was calculated in the

same way for leaf photosynthetic rate (Eqs. B9.2.16′ and B9.2.19′).

5. Sun–Shade Big-Leaf Model (SSM)

This model was developed by de Pury and Farquhar (1997). The sunlit fraction of leaf area index (LAI) is given by Eq. B9.2.28. Total PFD absorbed by sunlit leaves comprises direct, diffuse, and scattered direct light (Eq. B9.2.29). Total PAR absorbed by shaded leaves was obtained as the difference between PFD absorbed by the canopy and PFD absorbed by sunlit leaves (Eq. 9.2.30). Photosynthetic capacity of sunlit leaves expressed per unit ground area, $V_{cmaxt,su}$, was calculated as the integral of V_{cmax} of sunlit leaves, which was calculated as a function of leaf nitrogen content (Eq. 9.2.31). Photosynthetic capacity of shaded leaves was calculated as the difference between canopy photosynthetic capacity and the photosynthetic capacity of sunlit leaves (Eq. B9.2.32).

In calculation of all these models, CO_2 assimilation rates were calculated based on the biochemical model of Farquhar et al. (1980) as shown in Eqs. B9.2.16, B9.2.17, B9.2.18, B9.2.19, B9.2.20′, B9.2.21 and B9.2.22. Maximal carboxylation (V_{cmax}), maximal electron transport (J_{max}), and respiration rates (R_d) were assumed as linear functions of leaf nitrogen content per unit leaf area (N_l; Eqs. B9.2.23′, B9.2.24′ and B9.2.25′). Most parameters of leaf gas exchange were taken from data obtained from a wheat canopy (de Pury and Farquhar 1997). To evaluate the effects of interspecific variation in leaf traits, we adopted higher, middle, and lower values of the V_{cmax} to photosynthetic nitrogen ratio (a_V; 1.16, 0.58, and 0.29), corresponding roughly to PNUE of herbaceous, deciduous tree, and evergreen tree species (Hikosaka and Shigeno 2009; see Chap. 3, Hikosaka et al. 2016 for details of the gas exchange model).

The distribution of leaf photosynthetic nitrogen content was described with an exponential function (Eq. B9.2.15) and the slope (nitrogen distribution coefficient, k_b) was assumed to be half of the light extinction coefficient for diffuse light (Anten et al. 2000; K. Hikosaka, unpublished data; discussed below). However, as described in Box 9.1, BLM1 assumes that A_{max} is proportional to the relative PFD. This proportionality is achieved when the value of k_b is identical to that of the light extinction coefficient. Thus, BLM1 implicitly assumes that nitrogen distribution is steeper than that in other models.

The model simulation was performed for the vernal equinox day at the equator in which no cloud in the sky was assumed. Leaf temperature and intercellular CO_2 partial pressure were fixed at 21 °C and 25 Pa, respectively, meaning that the effect of stomatal limitation was not considered (see Sect. V for incorporating stomatal functions). Canopy photosynthetic rate was calculated every 30 min from dawn (0600) to dusk (1800) and daily carbon gain was obtained by the trapezoidal rule. The nighttime respiration rate is assumed to be twice as high as the day respiration rate (see Chap. 3, Hikosaka et al. 2016).

Figure 9.3 shows the light-response curves of canopy photosynthetic rate per unit ground area. BLM1 and BLM2 simulated a convex curve in which the rate was saturated at lower irradiance because this light response was identical to that in leaves. The difference in the light-saturated rate of canopy photosynthesis between BLM1 and BLM2 resulted from the difference in canopy nitrogen content. As mentioned above, BLM1 assumed a steeper nitrogen distribution than the other models, but the nitrogen content of top leaves was identical in all models so that total canopy nitrogen content was lower in BLM1 than in other models, leading to its lower canopy photosynthetic capacity.

The light response of the multi-layer models (MDDM and MSM) was less convex than that of the BLMs. This difference arose because light saturation of photosynthesis was not synchronized among layers;

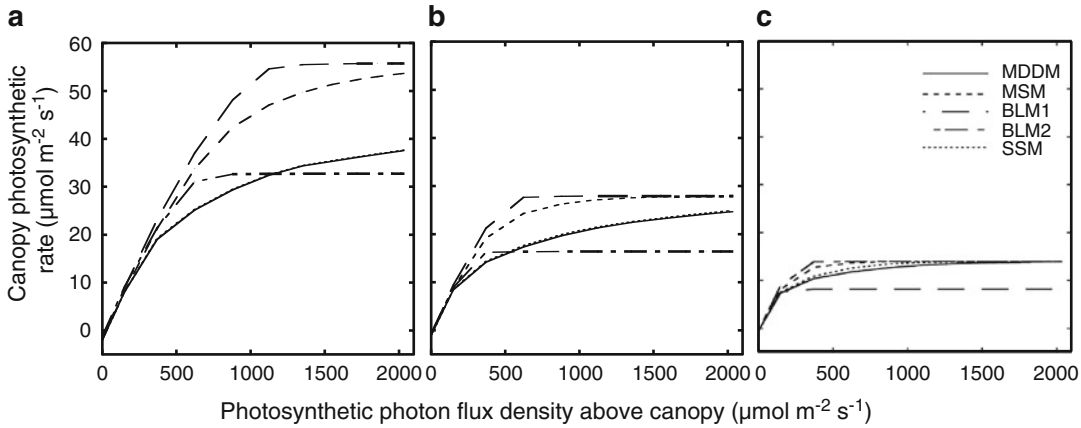

Fig. 9.3. Light-response curves of the canopy photosynthetic rate in five canopy photosynthesis models. MDDM, multi-layer model under direct–diffuse light; MSM, Multi-layer model with simple light extinction; BLM1 and BLM2, Big-leaf model 1 and 2; SSM, sun–shade big-leaf model. See text for detailed explanation of each model. Different levels of photon active radiation above the canopy assume the temporal PFD change from morning to noon in the cloudless vernal equinox day at the equator. Leaf angle was 45° in all models. Canopy nitrogen per unit ground area (N_t) was 400 mmol m^{-2} except for BLM1. In BLM1, leaf nitrogen content of the top layer (N_o) was identical to other models. The ratio of V_{cmax} to leaf photosynthetic nitrogen content (a_V) was 1.16, 0.58, and 0.29 × 10^{-3} s^{-1} in a, b, and c, respectively

photosynthesis in lower leaves was not saturated, whereas in upper leaves it was saturated (see Terashima and Saeki 1985). Canopy photosynthetic rate at high irradiance was higher in MSM than in MDDM. Furthermore, canopy photosynthetic rate in MDDM increased gradually, even at very high irradiance. These trends occurred because photosynthesis of all leaves was nearly light-saturated in MSM, but photosynthesis of shaded leaves in lower layers was not saturated in MDDM.

The light response of canopy photosynthesis in SSM was quite similar to that in MDDM. Give that SSM is a single-layer model, the computation effort is much lower than that in multi-layer models. Thus, SSM is a more accurate and useful morel.

The variation in the light-response of canopy photosynthesis among the five models was large when the V_{cmax} to photosynthetic nitrogen ratio a_V was high, but it was diminished when the ratio was small (Fig. 9.3). This is because most leaves were saturated at relatively lower irradiance when a_V is low. Therefore, the error in BLMs associated with ignoring direct light, may increase with the photosynthetic nitrogen-use efficiency of the plants considered.

IV. Effect of Canopy Traits on Canopy Photosynthesis

In addition to the effects of environmental factors, canopy photosynthesis of a given vegetation stand depends on the characteristics of the canopy. CPMs can analyze the dependencies of canopy photosynthesis on such characteristics as total leaf area index, light extinction, total leaf nitrogen in the canopy, nitrogen distribution among leaf layers, and leaf photosynthesis, including environmental response and nitrogen use (a_V). Environmental response of leaf photosynthesis is described in Chap. 3 (Hikosaka et al. 2016). The decrease in a_V results in a decrease in the maximum rate of canopy photosynthesis (Fig. 9.3). Here we analyze effect of other variables on canopy photosynthesis using MDDM.

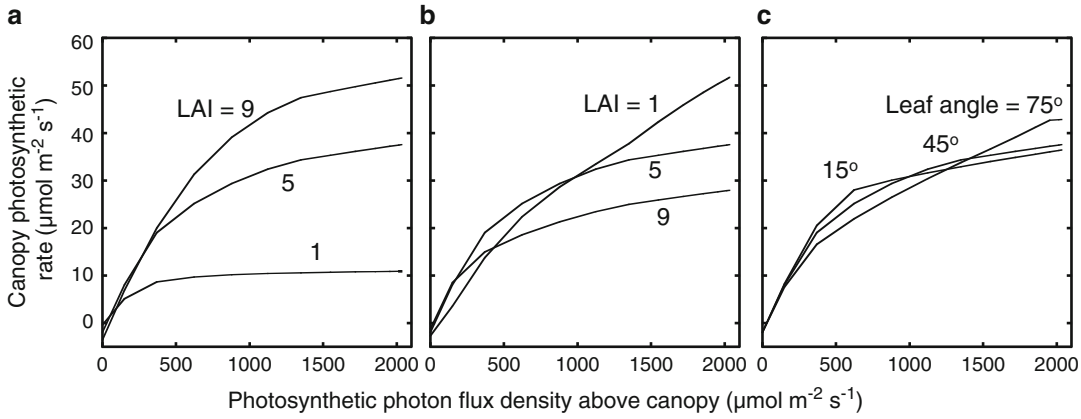

Fig. 9.4. Light-response curves of the canopy photosynthetic rate in the multi-layer model under direct–diffuse light (MDDM). (**a**) Leaf area index (LAI) was different with constant mean leaf nitrogen content per unit leaf area ($N_l = 80$ mmol m^{-2}); (**b**) LAI was different with constant canopy nitrogen content per unit ground area ($N_t = 400$ mmol m^{-2}); and (**c**) leaf angle was different. In a and b, leaf angle was 45°. In c, LAI and N_t was 5 m^2 m^{-2} and 400 mmol m^{-2}, respectively. The ratio of V_{cmax} to leaf photosynthetic nitrogen content (a_V) was 1.16×10^{-3} s^{-1} in every case

Figure 9.4a and b shows the light-response curve of the photosynthetic rates of canopies with different leaf area indices. In Figure 9.4a, b, the mean leaf nitrogen content per leaf area N_l and total leaf nitrogen content in the canopy per unit ground area N_t were constant, respectively. When the mean N_l was constant, the canopy photosynthetic rate was higher in a canopy with higher LAI irrespective of light (Fig. 9.4a). This difference occurs mainly because of the greater light absorption at higher LAI. In contrast, when N_t was constant, the effect of LAI on canopy photosynthesis is not simple; the photosynthetic rate of canopy with lower LAI was higher at high irradiance, but lower at low irradiance, compared with a canopy with a higher LAI (Fig. 9.4b). This complex result is owed to a trade-off between leaf area and leaf nitrogen content. Give that total nitrogen content (N_t) is assumed to be fixed, mean leaf nitrogen content per area (N_l) decreases with increasing LAI. Under high light, increasing N_l is advantageous because leaves have higher photosynthetic capacity. Under low light, increasing N_l is not beneficial because photosynthesis is limited by light rather than by nitrogen (see also Anten et al. 1995b). Decreasing LAI decreases light absorption, which lowers canopy photosynthesis. Consequently, when nitrogen is limited, extremely high or low LAI is disadvantageous. Fig. 9.5 shows simulation results of daily carbon gain of a canopy in which both LAI and canopy nitrogen were altered. When canopy nitrogen content was fixed, there was an optimal LAI that maximizes daily carbon gain (Anten et al. 1995b; Hirose et al. 1997). The optimal LAI increased with increasing canopy nitrogen content (Anten et al. 2004). Optimal LAI is discussed in Chap. 13 (Anten 2016).

Figure 9.4c shows light-response curves of photosynthetic rate in canopies with different leaf angles. The canopy with more-horizontal leaves (15°) had higher photosynthetic rates at lower irradiance but lower rates at higher irradiance. The higher rates occurs because more-horizontal leaves absorb more light under the same irradiance, owing to the higher associated k values. However, as the light increases, horizontal leaves that are exposed to light become light-saturated and this saturation dampens the response of canopy photosynthesis to light. In contrast, vertical leaves let more light through to lower canopy layers where it is efficiently used for photosynthesis. Thus, light is more homogenously used by

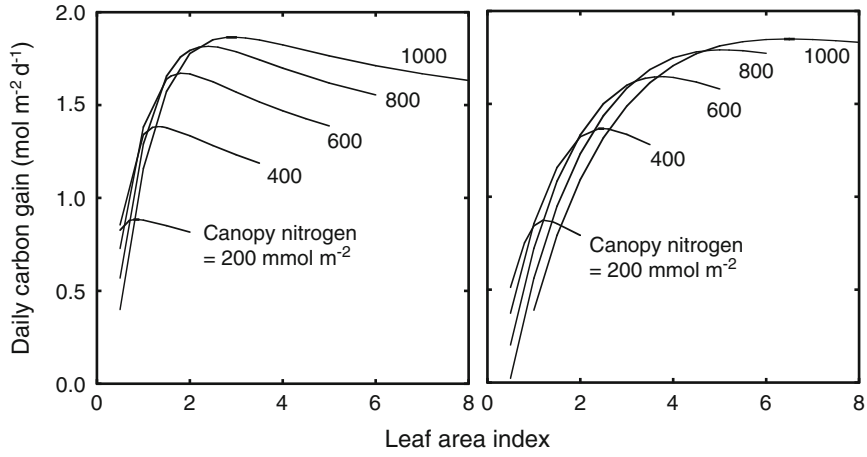

Fig. 9.5. Daily carbon gain as a function of leaf area index and canopy nitrogen content in a canopy with leaf angle of 15° (**a**) or 75° (**b**) in the multi-layer model under direct–diffuse light (MDDM). The ratio of V_{cmax} to leaf photosynthetic nitrogen content was 1.16×10^{-3} s^{-1}

different layers in the canopy. Compared at the same N_t, the optimal LAI was greater in a canopy with more vertical leaves (Fig. 9.5; Saeki 1960; Anten et al. 1995b).

Compared at the same N_t value, daily carbon gain of the canopy was similar between different leaf angles (Fig. 9.5). This result is inconsistent with simulation results of earlier models. For example, Saeki (1960) showed that maximal daily carbon gain was lower in canopies with higher k values (see also Hirose 2005). The result of Saeki (1960) was consistent with experimental results. For example, Tanaka (1972) manipulated the leaf inclination angle of a rice stand and found that canopy photosynthetic rate at high irradiance decreased with decreasing leaf angle (see also Monsi et al. 1973). Why does a canopy with horizontal leaves have low photosynthetic capacity in earlier studies? As mentioned above, earlier CPMs assumed a constant value for photosynthetic capacity. Thus, in a canopy with higher k values, photosynthesis of the topmost leaves is light-saturated, and absorbed light is not efficiently used for photosynthesis. Why then is canopy carbon gain similar between horizontal and vertical leaves in the present simulation? This is probably because we did not assume any constraint on increasing N_l or photosynthetic capacity. In this model, canopies with more horizontal leaves have steeper nitrogen distributions (higher k_b), leading to a higher N_l and associated light-saturated photosynthesis in upper leaves than those with more vertical leaves. However, the convexity of light-response curve of photosynthesis (θ, θ_j, or θ_{cj}), one of the other characteristics of the light-response curve of photosynthesis, often decreases with increasing N_l (Hirose and Werger 1987a; Hikosaka et al. 1999), which was ignored in the present model. Furthermore, increasing photosynthetic capacity of a leaf may be constrained by the availability of other resources such as water; if an increase in V_{cmax} is not accompanied by a proportionate increase in stomatal and mesophyll conductance, CO_2 concentration at the carboxylation site decreases. This response may lead to a smaller increase in photosynthetic capacity with an increase in leaf nitrogen content, and thus to a saturating relationship between photosynthetic capacity and leaf nitrogen content. To increase stomatal conductance, additional biomass may need to be invested in the root system to improve hydraulics. Otherwise, plants may suffer from a risk of water deficit in the leaf canopy (such as by embolism; see Chap. 7, Woodruff et al. 2016). Therefore, having very high leaf photosynthetic rates

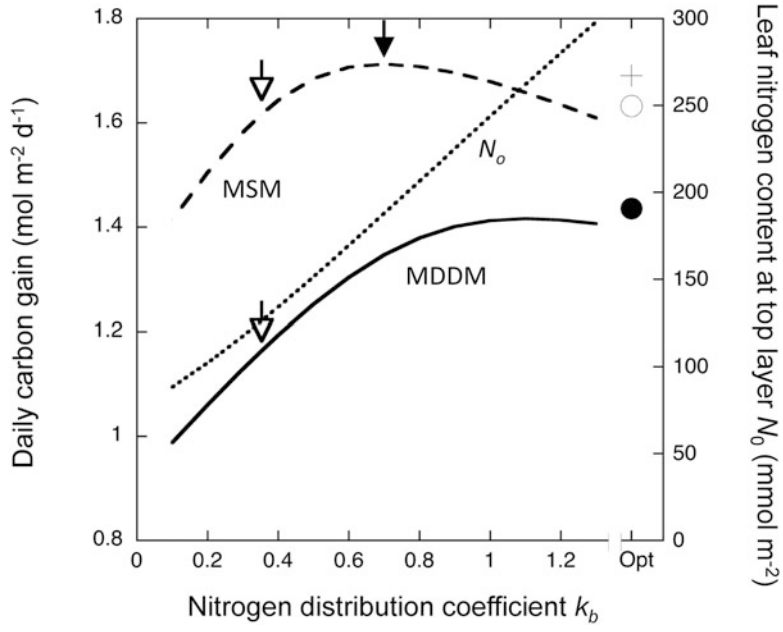

Fig. 9.6. Effects of nitrogen distribution on the daily carbon gain of the canopy. *Continuous* and *broken lines* denote carbon gain under direct–diffuse light and under diffuse light only, respectively, plotted against the nitrogen distribution coefficient (k_b). The *dotted line* describes leaf nitrogen content at the top layer. *Closed* and *open circles* show carbon gain of the canopy under direct–diffuse light and under diffuse light only, respectively, where nitrogen distribution is optimized under direct–diffuse light. The cross shows nitrogen content at the top layer in the canopy optimized under direct–diffuse light. *Open arrows* show carbon gain at actual nitrogen distribution, which is assumed to be half of k_{dif}. The *closed arrow* shows carbon gain when nitrogen distribution is optimized under diffuse light only. Redrawn from Hikosaka (2014)

may be costly. If water supply is saved, higher N content may be wasteful. Such constraints on increasing photosynthetic capacity lead to an upper limit of leaf nitrogen content, and horizontal leaves may be unable to achieve high canopy photosynthesis.

Figure 9.6 shows the effect of nitrogen distribution on daily carbon gain in as simulated by the MDDM and MSM (Hikosaka 2014). Open arrows denote the value of k_b (nitrogen distribution coefficient) observed in actual canopies (half of the light extinction coefficient; Anten et al. 2000, K. Hikosaka et al., unpublished data). Dependence of daily carbon gain on k_b was considerably different between MDDM and MSM. In MSM, daily carbon gain was maximized when the value of k_b was the same as that of the light extinction coefficient. When k_b was optimal in MSM, nitrogen content was proportional to light availability (Anten et al. 1995a; see Chap. 13, Anten 2016 for details). In contrast, optimal k_b in MDDM was much higher than that in MSM. MSM assumes that light availability is identical among leaves within the same canopy layer. Thus, plants can allocate an appropriate amount of nitrogen to leaves so that the nitrogen content is proportional to light availability. In contrast, under direct–diffuse light conditions, some leaves receive both direct and diffuse light, whereas others receive only diffuse light. Furthermore, light availability of a leaf fluctuates depending on the solar position and other factors, leading to optimal nitrogen allocation being different from that shown in MSM.

V. Canopy Photosynthesis Models with Heat Exchange

CPMs described above can simulate CO_2 exchange rates as a function of environmental variables. However, these models need

leaf temperature and intercellular CO_2 partial pressure C_i (or stomatal conductance) as input data (note that simulations in Sect. IV used fixed leaf temperature and C_i). Furthermore, leaf temperature generally differs from air temperature as a result of energy exchanges in the surroundings. For this reason, a complete canopy photosynthesis model needs to incorporate energy balances.

The surface energy balance for both an individual leaf surface and a vegetated land surface is:

$$R_{\mathrm{S\_ab}} + R_{\mathrm{L\_ab}} - R_{\mathrm{L\_out}} = H + \lambda E + G \quad (9.2)$$

where R_{S_ab} and R_{L_ab} are total solar and thermal radiation absorbed by leaves and bulk vegetation surface, respectively, R_{L_out} is outgoing thermal radiation from a surface, H and E are sensible heat and water vapor fluxes from this surface, respectively, λ is the latent heat of vaporization of water, and G is the heat flux into thermal storage depending on surface temperature (T_c) in a way that can be determined precisely only by solving the heat diffusion equation. At the leaf-scale, R_{S_ab} and R_{L_ab} are the computation results from the formulation of radiative transfer within the canopy (see Kumagai et al. 2006). In contrast, on land surface-scale, R_{S_ab} is calculated as $(1 - a_l) \times R_S$, where a_l is the albedo (the reflection of solar radiation) and R_S is solar radiation, and incident thermal radiation can be substituted for R_{L_ab}. R_{L_out} is expressed as a function of T_c according to the Stefan–Boltzmann law at the leaf-scale. Two-sided evolution and probability of no contact within a given canopy layer must be considered (see Kumagai et al. 2006).

When we consider heat balance in each canopy layer, H and λE depend on T_k, and from a leaf surface, giving:

$$H = 2\Delta L m_a c_p g_H (T_k - T_a) \quad (9.3)$$

$$\lambda E = \lambda \Delta L m_e g_E \frac{e_{\mathrm{sat}}(T_k) - e}{P} \quad (9.4)$$

where ΔL is the LAI in a given canopy layer, m_a and m_e are the molecular weights of air and water, respectively, c_p is the specific heat of air at constant pressure, g_H and g_E are the leaf-scale heat and the vapor conductances, respectively, T_k and T_a are the leaf and air temperatures, $e_{sat}(T_k)$ and e are the saturation vapor pressures at T_k, which can be represented by a function of T_k, and atmospheric water vapor pressure, respectively, and P is the atmospheric pressure.

Equations 9.2, 9.3, and 9.4 are to be solved for one unknown, individual leaf-scale T_k. As may be seen, the T_k is among the most critical factors in computing both biological and physical aspects in the atmosphere-leaf exchange models. For example, the T_k influences a computation result of leaf-scale photosynthetic rate (A) via computation of biocatalytic reactions in the photosynthesis model, and thus, controls the stomatal conductance (see Chap. 3, Hikosaka et al. 2016). Also, T_k modulates the turbulent heat and moisture transfer by controlling thermal convection above the leaf surface, resulting in alteration of the leaf boundary layer conductance. Because H and λE in Eq. 9.2 are altered through these processes, the energy balance model (Eq. 9.2) with the flux models (Eqs. 9.3 and 9.4), the photosynthesis coupled with stomatal conductance model, and the boundary layer conductance model taking into consideration the effects of both forced and free convection (see Campbell and Norman 1998), must be solved simultaneously for all unknowns by numerical iteration.

When we consider the whole vegetation, fluxes from a vegetation surface are given by:

$$H = \rho c_p g_{Ht} (T_k - T_a) \quad (9.5)$$

$$\lambda E = \frac{c_p \rho}{\gamma} g_{Et} (e_{sat}(T_k) - e) \quad (9.6)$$

where ρ is the density of air, γ is the psychrometric constant, T_k is canopy-scale leaf temperature and g_{Ht} and g_{Et} are the canopy-scale heat and the vapor conductances, respectively. Note that the reciprocal of the total conductance is the sum of the reciprocals of the component conductances, namely the stomatal and boundary layer conductances.

Equations 9.2, 9.5, and 9.6 are formulations from a BLM (see Sect. III.B) to be solved for one unknown, canopy-scale T_k. Practically, the T_k is the canopy surface temperature denoting radiative temperature above the canopy, which can be derived using observed upward long-wave radiation and inversion of the Stefan–Boltzmann equation. Thus, note that the canopy-scale T_k cannot be related to the leaf-scale T_k by a simple equation. However, as with the leaf-scale T_k, the canopy-scale T_k alters a computation result of canopy-scale A and stomatal conductance, resulting in modifications of surface energy partitioning (i.e., H and λE) and atmospheric stability above the canopy.

Hence, we can define local feedbacks between the T_k formation and the atmosphere-land fluxes including a carbon flux such as A. Among the feedbacks, this section discusses "aerodynamic feedback," impacts of atmospheric convective motion induced by the T_k formation on the fluxes using canopy-scale theory (Raupach 1998). It should also be noted that when the leaf-scale theory is used, formulations describing fluxes within atmospheric surface layers (see Chap. 10, Kumagai 2016) are almost the same between the two theories. As mentioned above, g_{Et} (and also the canopy-scale CO_2 conductance, g_{Ct}) can be represented as:

$$\frac{1}{g_{Et}} = \frac{1}{g_{at}} + \frac{1}{g_{st}} \tag{9.7}$$

where g_{at} is the aerodynamic conductance, and g_{st} is the canopy stomatal conductance, whose formulation is described in Chap. 2 (Gutschick 2016). For computing g_{Ct}, g_{at} and g_{st} should be adjusted to be appropriate for the CO_2 transfer. g_{at} is usually expressed using Monin-Obukhov similarity theory (Garratt 1992):

$$g_{at} = \frac{\kappa^2 u}{\chi_H(z-d, z_{0H}, l)\chi_M(z-d,\ z_{0M}, l)} \tag{9.8}$$

where κ is the von Karman constant, u is wind velocity measured at a height of z, χ_H and χ_M are dimensionless temperature and velocity profiles, respectively, d is the zero-plane displacement, z_{0H} and z_{0M} are the roughness lengths for heat and momentum, respectively, and l is the Monin-Obukhov length. The aerodynamic feedback denotes the modulations of turbulent heat and moisture transfer by alteration of g_{at} through atmospheric stability (l) and thereby through the surface energy balance (Eq. 9.2), feeding back on Eq. 9.2 itself (Raupach 1998).

Raupach (1998) incorporated the convective boundary layer (see Chap. 10, Kumagai 2016) slab model (McNaughton and Spriggs 1986) into the surface energy balance model (Eq. 9.2) and investigated the impact of aerodynamic feedback on computations of water vapor and CO_2 fluxes (Fig. 9.7). Here, the effect of soil water stress on photosynthetic rate (s_W values in Fig. 9.7) was also considered. Without aerodynamic feedback, surface temperature reaches up to around 40 °C even under the moistest conditions, and the high surface temperature reduces the magnitudes of water vapor and CO_2 fluxes through the effect of stomatal closure in the hottest part of the day. When aerodynamic feedback is considered, turbulent heat and moisture transfer enhanced by unstable stratification induces a cooling effect on the surface, resulting in attenuating the tendency to heat-induced stomatal closure. Thus, assessing and describing surface temperature formation and the atmospheric convective motion above the surface are necessary for building a canopy exchange model.

VI. Validation

A. Plant Growth and Model Prediction

Given that assimilated carbon that is not respired is utilized for plant growth, we can test the validity of predicted gas exchange rates by comparing them with plant growth rates. Previous studies have shown that the estimated canopy carbon exchange rate is closely related to plant growth rate.

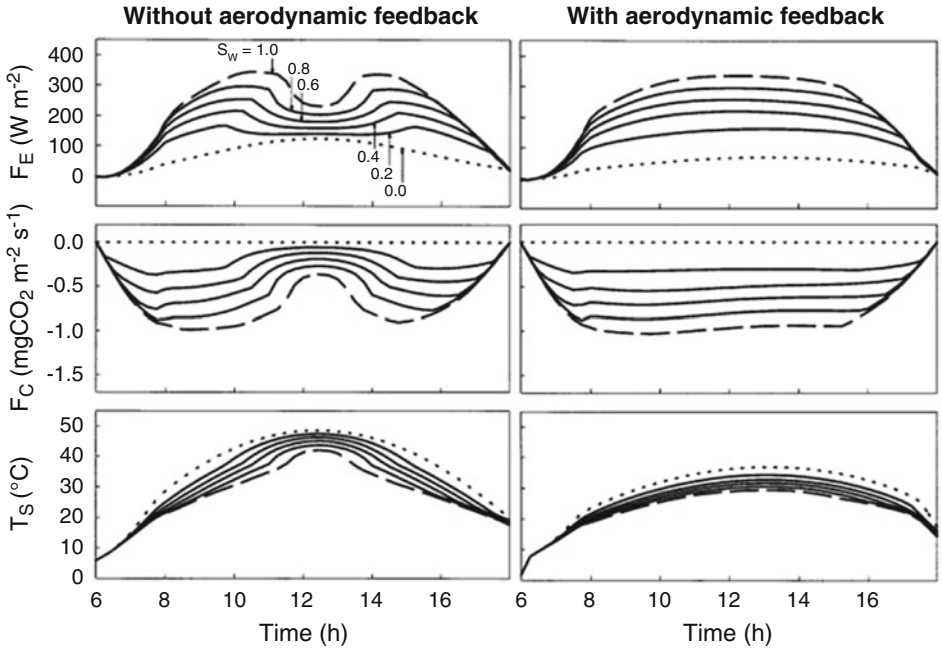

Fig. 9.7. Temporal variations in water vapor (F_E) and CO_2 (F_C) fluxes, and surface temperature (T_S) computed by the surface energy balance model incorporated into the convective boundary layer slab model without (*left panels*) and with (*right panels*) aerodynamic feedback. Different curves represent different values of water stress parameter s_W, which can vary between 0 (highly water-stressed) and 1 (least water-stressed). Redrawn from Raupach (1998 with modification)

For example, Hirose et al. (1997) established stands of annual plants under two CO_2 concentrations in greenhouses with natural sunlight. Although they did not determine the respiration rates of stems and roots, canopy photosynthetic rates estimated with MSM (multilayer model using simple light extinction) were significantly correlated with stand growth rates. Borjigidai et al. (2009) established stands of *Chenopodium album* under two CO_2 concentrations using open-top chambers. Growth rates were estimated using biomass and dead parts of plants harvested four times during the growing season. Canopy photosynthesis was estimated using MSM with environmental variables determined near the open-top chambers and respiration rates of stems and roots were determined. The estimated carbon balance was not only strongly correlated but also showed a 1:1 relationship with stand growth (Fig. 9.8a), suggesting that CPMs predict quantitatively correct rates of CO_2 exchange rates. See also Chap. 12 (Ohtsuka et al. 2016) for the case of a forest ecosystem.

CPMs are useful for estimation of carbon exchange of individuals in a plant stand (See Chap. 14, Anten and Bastiaans 2016 for their principle). Hikosaka et al. (1999, 2003) estimated growth rates of aboveground part of individuals in a dense stand of annual plants using allometric relationships between size and mass of individual plants. The calculated plant growth rates were strongly correlated with leaf daily carbon gain of individuals (Fig. 9.8b), suggesting that CO_2 exchange rates can also be estimated correctly even at an individual level.

B. Eddy Covariance and Model Prediction

Measurements of CO_2 flux by the eddy covariance method allow us to examine terrestrial carbon cycle models in terms of canopy- and ecosystem-scale net carbon

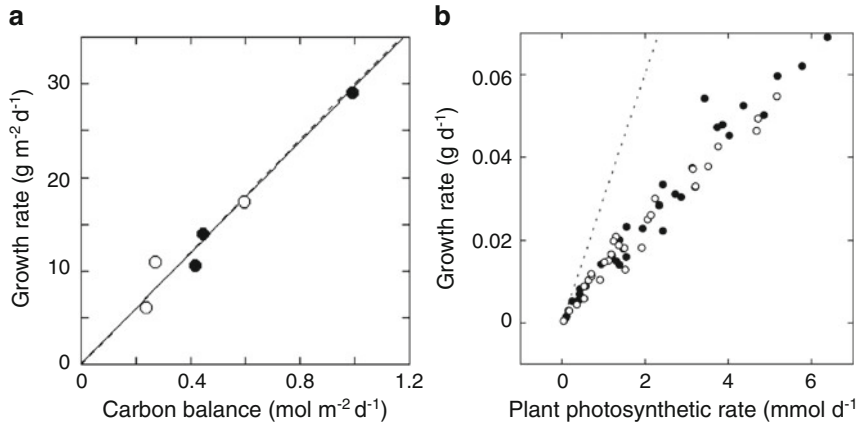

Fig. 9.8. Comparison between plant growth and estimated carbon balance. (**a**) Growth rate per unit ground area of *Chenopodium album* stands as a function of estimated daily carbon balance (canopy photosynthesis minus respiration). Stands were established at two CO_2 concentrations (*open* and *closed circle* denotes ambient and 700 μmol mol^{-1}, respectively). The plant density was 93 m^{-2} and top leaves of all individuals were exposed to the canopy top. The whole plant body was harvested four times and the growth rate for each interval was determined. Carbon balance was calculated as a mean of the interval. See Borjigidai et al. (2009) for details. (**b**) Growth rate of individuals in *C. album* stands as a function of estimated daily carbon gain. Stands were established at two CO_2 concentrations (*open* and *closed circles* show ambient and 700 μmol mol^{-1}, respectively). The plant density was 400 m^{-2} and there was a large variation in plant size. Aboveground mass of each individual in the census quadrat was estimated in the first census using the allometric relationship of length and diameter of stems and aboveground mass of harvested individuals from another quadrat. In the second census aboveground part of individuals in the census quadrat was estimated. Carbon gain was estimated as average for leaves of each individual in the two census (allocation of assimilates to stems and roots was not considered). See Hikosaka et al. (2003) for details

budget at fine temporal resolutions (see Chap. 10, Kumagai 2016). The eddy-covariance method directly measures net ecosystem CO_2 exchange (NEE), which can be separated into photosynthetic and respiratory components on the basis of the nighttime temperature–NEE (respiration only) relationship (Reichstein et al. 2005). Thus, it is possible to compare gross primary production (GPP, which is essentially same as the gross canopy photosynthesis), ecosystem respiration (RE), and NEE (= GPP − RE) between model estimations and flux measurements at typically 30-min time steps. Until the mid-1990s, it was impossible to evaluate NEE directly; in most cases, field-measured net primary production (NPP) and carbon stock data at annual time steps were used for model validation. Development of the flux measurement method allowed model validation in a novel and more accurate manner. At present, flux measurement sites constitute a worldwide network, called FLUXNET (Baldocchi et al. 2001); 732 sites as of July 2015. Since the establishment of the first tower site in Harvard Forest, U.S., in 1992, more than 20 years of records have accumulated and are accessible to researchers, allowing us to explore not only micrometeorological but also ecological aspects of CO_2 fluxes (Baldocchi 2008).

Although increasing amounts of flux measurement data are available, several limitations should be considered when model validation is performed with these data. First, there are some biases and errors associated with measurements by the eddy covariance method, especially during nighttime and in mountainous areas, owing to hilly terrain. The fundamental micrometeorological theory on which the eddy covariance method is based was developed for a sufficiently turbulent condition over a flat

surface and cannot adequately consider the effect of advection (transport by air mass flow). Second, the quality of flux data depends heavily on the methods used for bias correction, data selection, and gap-filling. For example, Papale et al. (2006) showed that threshold friction velocity of wind (u^*, an index of atmospheric turbulence) is one of the critically important factors for data selection and quality. Third, the spatial scale usually differs between the ecosystem model and the flux measurement. In general, the upwind area contributing to the flux measured by instruments (in micrometeorology, this area is called a footprint) depends on wind condition and covers up to a few square kilometers (km^2), whereas ecosystem models are often applied to broader areas. In particular, the spatial resolution of global terrestrial ecosystem models is typically hundreds to thousands of km^2 (e.g., $0.5^\circ \times 0.5^\circ$, a typical global-model grid size, covers about 3000 km^2 on the equator) often containing diverse land cover types. In addition, the footprint of flux measurement varies with wind direction. Accordingly, when flux data are used for model validation, care about such data limitations and scale-gaps is essential.

During the last 10 years, more and more studies have used flux measurement data for validation of terrestrial carbon cycle models including CPMs. Sitch et al. (2003) validated the LPJ dynamic global vegetation model at six sites in Europe. Krinner et al. (2005) validated the ORCHIDEE model at 28 sites in Europe, not only for NEE but also for energy exchange fluxes. Ito et al. (2005) and Sasai et al. (2005) applied the VISIT and the BEAMS models, respectively, to the Takayama flux measurement site in Japan; Fig. 9.9 shows examples of the site-scale validation using flux measurement data.

Recently, flux measurement data have been used for model validation in other ways as well, especially as benchmarking data for model intercomparison. Several studies have compared ecosystem models at multiple sites (e.g., Kramer et al. 2002; Morales et al. 2005; Schwalm et al. 2010; Richardson et al. 2012; Ichii et al. 2013). These studies indicated that the present models worked poorly in several regions;

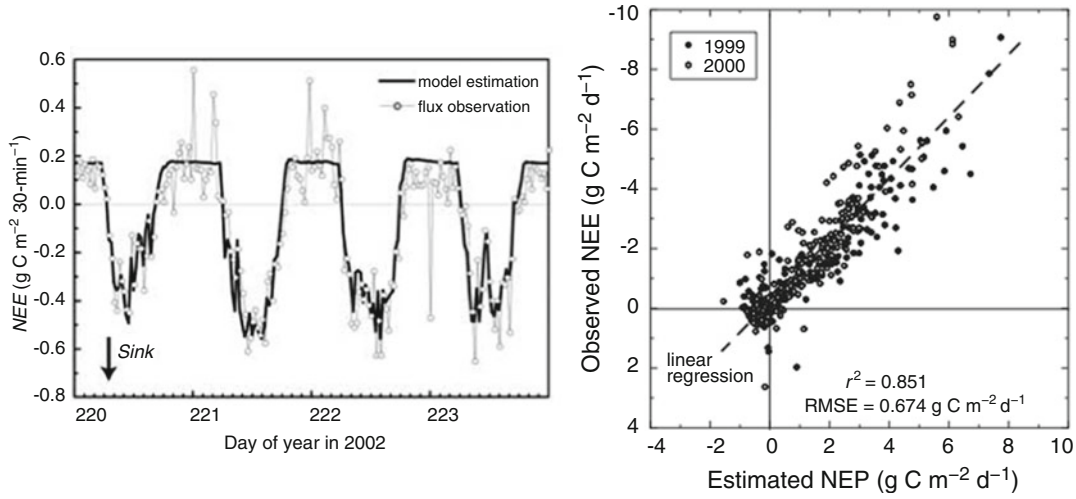

Fig. 9.9. Comparison of net CO_2 exchange (NEE) between eddy-covariance measurement and model estimation at the Takayama site. A process-based terrestrial ecosystem model, VISIT (Ito et al. 2006), was applied to the site, using the sun–shade canopy scheme of de Pury and Farquhar (1997). (*Left*) Time-series of 30-min step simulation in mid-summer of 2002, and (*right*) 1:1 comparison for daily NEE in 1999 and 2000. Note that seasonal change in leaf photosynthetic parameters is included in an empirical manner

for example, Morales et al. (2005) showed that most models failed in simulating CO_2 fluxes at Mediterranean sites, where water stress is a key factor. Also, these comparison studies are effective for identifying key processes. For example, Richardson et al. (2012) suggested that the present ecosystem models have difficulty in simulating leaf phenology.

These validations show that the present models have improved in capturing canopy photosynthesis in various ecosystems. Incorporating biochemical photosynthesis models and canopy radiation models (mentioned above) into ecosystem models make them highly mechanistic, allowing researchers to interpret observational data from an ecophysiological point of view and to conduct various sensitivity analyses to identify key parameters. However, it is also apparent that uncertainties remain in the present models, as implied by model intercomparison studies. As shown by the canopy-model comparison (Fig. 9.3), differences in model structure, parameter values, and assumptions can result in remarkably different simulation results. To improve simulation credibility, we need further refinement of process models including CPMs and broad-scale validation using data from multiple sites.

VII. Application of Canopy Photosynthesis Models to Larger Scales

Because quantification of primary productivity of the biosphere has received much interest from ecologists and geochemists, many researchers have attempted to evaluate global GPP and NPP (Ito 2011). For example, the International Biological Programme (IBP, 1965–1972) collected a large number of field data of NPP from various ecosystems and estimated global total NPP. During the IBP period, empirical models (statistical regression) were used; for example, the Miami model estimates annual NPP of any terrestrial ecosystems as a function of annual mean temperature and annual precipitation (Lieth 1975). Although these models captured the geographic variability of mean annual NPP well, they were unable to simulate seasonal and interannual variability and environmental impacts, such as for land-use change.

During the last few decades, global environmental issues have gained increasing awareness from the general public and scientific community as one of the urgent issues. In particular, temporal variability and spatial heterogeneity of the carbon cycle, including terrestrial CO_2 uptake has received attention from many researchers. Accordingly, canopy or vegetation models have been used at large spatial scales, including the global scale. Table 9.2 summarizes the canopy parameterization approaches used in several global terrestrial ecosystem models. Additionally, several recent models have adopted individual-based approaches to simulating vegetation dynamics (e.g., Levy et al. 2004; Sato et al. 2007) in conjunction with some photosynthetic scheme. Because observational data of ecosystem properties are quite limited at these scales, the models are expected to work at as little input of a priori information as possible. As mentioned above, empirical models have been widely used to estimate terrestrial primary productivity. During the early period of global studies (the 1980s and early 1990s), only a few datasets of global climatology and land cover were available. In the 1990s, many different kinds of global terrestrial models were developed in accordance with the increase of global datasets.

In particular, global satellite remote sensing data became available, enabling us to evaluate vegetation activity at broader scales. Importantly, Monteith (1977) developed a fundamental relationship between canopy-observed solar energy and vegetation productivity; the conversion coefficient was termed light-use efficiency (LUE; carbon exchange per unit absorbed light). Using the satellite-derived vegetation absorption of solar energy (PFD) and the LUE principle, it was possible to estimate NPP by remote

Table 9.2. Summary of canopy schemes in several global terrestrial ecosystem models

Model	Biome-BGC	CASA	CLM ver.4	LPJ	ORCHIDEE	VISIT
References	Running and Hunt (1993)	Potter et al. (1993)	Bonan et al. (2011)	Sitch et al. (2003)	Krinner et al. (2005)	Ito et al. (2005)
Canopy structure	Mono-layer	Mono-layer	Mono-layer (tree/grass)	Mono-layer (tree/grass)	Mono-layer (tree/grass)	Overstory/understory
Leaf photosynthesis	Asymptotic light-response curve	Light-use efficiency model	Biochemical model (Farquhar)	Biochemical model (Haxeltin and Prentice)	Biochemical model (Farquhar)	Biochemical model (Farquhar)
Scaling-up method	Big-leaf	Big-leaf	Sun/shade, N distribution	Optimal leaf N distribution	Optimal leaf N distribution	Sun/shade, N distribution
C_3/C_4 plants	No	No	Yes	Yes	Yes	Yes
Stomata	Nobel	No	Ball et al.	Haxeltin and Prentice	Ball et al.	Leuning

sensing. Since 1982, continuous monitoring data of global terrestrial vegetation are available such as NOAA-AVHRR, Terra/Aqua-MODIS, and SPOT-VEGETATION for the purposes of various analytical and modeling studies. Time-series of vegetation indices (e.g., NDVI, Normalized Difference Vegetation Index) have revealed seasonal and interannual variation of vegetation activity (Myneni et al. 1997; Nemani et al. 2003). The vegetation indices are also useful for characterizing the photosynthetic properties of vegetation stands. For example, Sellers (1985) estimated the fraction of canopy-absorbed PFD from the simple ratio of visible red to near-infrared reflectance. Subsequently, Potter et al. (1993) adopted this approach and developed a new terrestrial ecosystem model, the Carnegie-Ames-Stanford Approach (CASA). Similar methodology was employed by several models (e.g., Ruimy et al. 1996; Goetz et al. 1999). These models are simple and reasonably capture the present vegetation productivity. However, they have several shortcomings: (1) these models are driven by satellite-observed data and so are not applicable for future projections; (2) it is difficult to include ecophysiological findings to improve this kind of model, although Sasai et al. (2005) has developed a mechanistic satellite-driven model. More recently, new sensors, such as synthetic aperture radar and lidar, are used to assess canopy structure from the space.

To improve future projections, process-based models of terrestrial ecosystems are effective because these models consider ecophysiological factors such as different environmental responsiveness between C_3 and C_4 plants. Several process-based models have been developed on the basis of stand-scale carbon cycle models and tested using field data. Running and Hunt (1993) developed a global model, the Biome-BGC, on the basis of the Forest-BGC model developed for pine forest studies in Montana, U.S. Similarly, Ito and Oikawa (2002) developed the Simulation model of Carbon cYCle in Land Ecosystem (Sim-CYCLE) on the basis of a carbon cycle model that was developed for tropical forest studies in Pasoh, Malaysia. Figure 9.10 shows the global annual NPP and its water-use efficiency estimated by VISIT (Ito and Inatomi 2012), developed from Sim-CYCLE. Earlier global terrestrial models adopted the "big-leaf" canopy approach for simplicity, and it is notable that these models are able to predict LAI and estimate impacts of environmental change. For global application, these models should estimate leaf phenology in deciduous forests and grasslands, which is determined by temperature, water, and radiation (for example, day-length) conditions. Many models include some phenological scheme, in which leaf seasonal display and shedding occur on the basis of cumulative temperatures above/below certain threshold

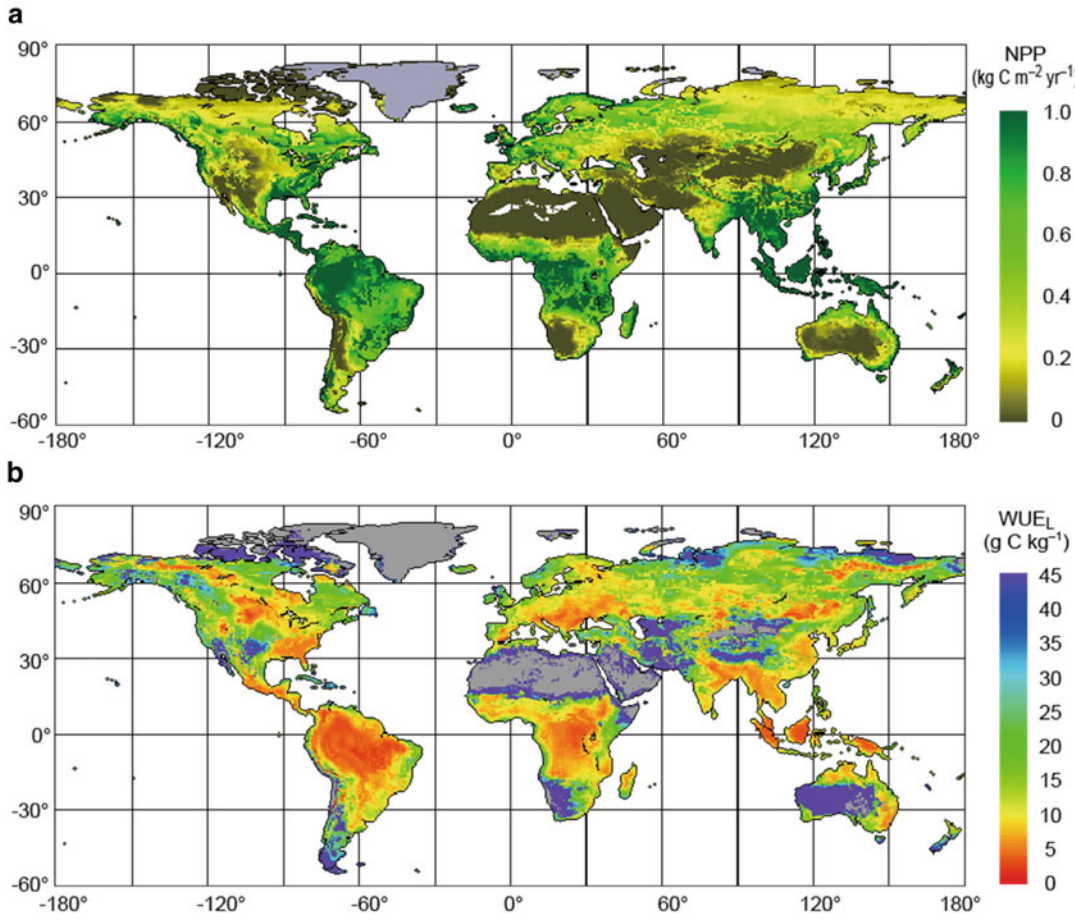

Fig. 9.10. Global distribution of (**a**) net primary production (NPP) of terrestrial ecosystems and (**b**) water-use efficiency (WUE, carbon assimilation per unit later loss) in 1995–2004, estimated by VISIT model (Ito and Inatomi 2012)

temperatures. The "big-leaf" scheme in earlier process-based models considers vertical attenuation of PFD within canopy but in most cases neglects the difference between direct and diffuse radiation as discussed earlier (see Sect. III.B. BLM). Using the Monsi–Saeki theory, leaf-level photosynthesis is integrated to canopy-level gross primary production (GPP), considering environmental factors (ambient CO_2, temperature, and moisture) in empirical but ecophysiological ways. For example, the leaf modules estimate stomatal conductance using several semi-empirical models (e.g., Ball et al. 1987; Leuning 1995; see Chap. 3, Hikosaka et al. 2016), which respond directly to atmospheric humidity and CO_2 concentration. A similar approach was adopted by land-surface parameterization schemes (such as the second version of Simple Biosphere [SiB2]; Sellers et al. 1997) used in climate models, which need to estimate surface energy and gas exchange including stomatal regulation. In most cases, the temperature and moisture limitations were included by developing empirical scholar functions (i.e., multipliers; from zero under severe conditions to one under standard condition) for maximum photosynthetic rate. Because terrestrial models differ in canopy integration (for example, assumption of light attenuation coefficient) and

environmental functions, their simulation results are not always consistent, implying estimation uncertainty.

Since the late 1990s, advances in CPMs have made it easier to conduct simulations of global terrestrial production and the carbon cycle. On the other hand, model validations in comparison with observation data have indicated that there remain large uncertainties and insufficiencies in the present models. One evident example is the anomalous CO_2 uptake after the huge eruption of Mt. Pinatubo, Philippines, in June 1991. After the eruption, a massive amount of volcanic ash was ejected into the atmosphere, as far as to the stratosphere, resulting in unusual scattering of solar radiation. This event was associated with anomalous cooling of Earth's surface by about 0.5 °C, affecting terrestrial ecosystems including croplands. Simultaneously, the atmospheric CO_2 growth rate slowed down notably, but the mechanism causing this slowdown has not been clear. Several model studies implied a reduction of respiratory emissions due to cooling, but it was insufficient to explain the phenomenon fully. Gu et al. (2003) pointed out that net CO_2 uptake of the Harvard Forest increased apparently after the Mt. Pinatubo eruption and proposed a hypothesis that increase of diffuse radiation after the event enhanced photosynthetic CO_2 uptake by the vegetation canopy at broad scale (Roderick et al. 2001). Because the "big-leaf" canopy scheme could not evaluate the effect of different radiation components (direct and diffuse radiation), the anomalous event enhanced use of the more mechanistic canopy radiation transfer and photosynthetic scheme to adequately capture the interannual variability of terrestrial CO_2 budget. Also, Mercado et al. (2009) implied that the diffuse-radiation fraction would increase as a result of human-emitted aerosols, indicating the importance of an improved canopy scheme for global terrestrial ecosystem models. Accordingly, several recent terrestrial models employ sun–shade canopy schemes (SSM) to include biochemical photosynthetic responses and canopy absorption of direct–diffuse light as discussed in Sect. III.

More than 30 terrestrial ecosystem models applicable to global scale have been developed. They are used for simulating not only current states but also past and future changes in response to environmental change. Process-based models are expected to work reasonably well under different conditions because they take account of ecophysiological factors (such as CO_2 fertilization effects on photosynthesis) determining ecosystem responsiveness. For example, Melillo et al. (1993) estimated that global NPP would increase by about 20 % under doubled atmospheric CO_2 and climate change condition using the Terrestrial Ecosystem Model (TEM). More recently, Friend et al. (2014) assessed the future change in vegetation carbon budget on the basis of simulation results of seven terrestrial ecosystem models.

As shown in Table 9.2, current terrestrial models adopt different canopy schemes in terms of complexity and environmental responsiveness. Another important feature is the inclusion of nitrogen effects on canopy photosynthesis. Using the model sensitivity analysis, Friend (2001) found that realistic nitrogen allocation should be taken into account for improving model simulations, in comparison with classical "big-leaf" models. This finding is consistent with field-scale ecophysiological and modeling studies (e.g., Hirose and Werger 1987b; Hikosaka 2014). The current models differ in approach and complexity in parameterization of canopy processes (Table 9.2), leading to considerable intermodel difference in estimated results. For example, Cramer et al. (1999) compared global terrestrial NPP estimated by 17 models and found that the results ranged from 39.9 to 80.5 Pg C $year^{-1}$ (Pg = 10^{15} g), even using common input climate data and simulation protocols. Such estimation uncertainty has not been reduced until recently. In the Multi-scale Terrestrial Model Intercomparison Project (MsTMIP; Huntzinger et al. 2013), it was found that 10 terrestrial models

differ in estimates of global terrestrial NPP from 36 to 67 Pg C $year^{-1}$ at the present time. A similar range of variability was also found among the terrestrial models embedded in Earth System Models (Todd-Brown et al. 2013), which are used for climate projection. Apparently, such uncertainty exerts serious influences on future projections under global environmental change, including the climatic feedback by the terrestrial biosphere through CO_2 exchange. Further studies are needed to improve vegetation canopy models and to reduce estimation uncertainty.

VIII. Conclusion

Current CPMs can predict land–atmosphere exchange rates of carbon, water, and energy almost correctly. Not only detailed models but also simplified models, some of which provide quite accurate predictions, have been developed. Scaling up from leaf to canopy level contributes to the understanding of mechanisms that cause variation in canopy exchange rates of gas and energy. CPMs also contribute to future projections of responses in ecosystem functions to future global climate change. For accurate prediction, however, we need detailed information of plant traits such as LAI, light extinction coefficient, leaf biochemical characteristics, and vertical variation in leaf traits, all of which vary considerably between species and as a function of environmental factors. Since part of environmental responses of such plant traits are not fully known, some projections involve large uncertainties. The increasing amounts of flux measurement data, ecophysiological findings, and the improvement of data–model fusion, especially in a collaborative manner, will bring new and deeper insights and eventually allow advanced prediction.

Acknowledgments

We thank Niels Anten for valuable comments. This work was supported by Grants-in-Aid for Scientific Research on Innovative Areas (Nos. 21114009 and 21114010), by KAKENHI (Nos. 20677001, 25291095, 20323503 and 25660113) and by CREST, JST, Japan.

References

Amthor JS (1994) Scaling CO_2-photosynthesis relationships from the leaf to the canopy. Photosynth Res 39:321–350

Anten NPR (1997) Modelling canopy photosynthesis using parameters determined from simple non-destructive measurements. Ecol Res 12:77–88

Anten NPR (2016) Optimization and game theory in canopy models. In: Hikosaka K, Niinemets Ü, Anten N (eds) Canopy Photosynthesis: From Basics to Applications. Springer, Berlin, pp 355–377

Anten NPR, Bastiaans L (2016) The use of canopy models to analyze light competition among plants. In: Hikosaka K, Niinemets Ü, Anten N (eds) Canopy Photosynthesis: From Basics to Applications. Springer, Berlin, pp 379–398

Anten NPR, Hirose T (2003) Shoot structure, leaf physiology and carbon gain of species in a grassland. Ecology 84:955–968

Anten NPR, Werger MJA (1996) Canopy structure and nitrogen distribution in dominant and subordinate plants in a dense stand of *Amaranthus dubius* (L.) with a size hierarchy of individuals. Oecologia 105:30–37

Anten NPR, Schieving F, Werger MJA (1995a) Patterns of light and nitrogen distribution in relation to whole canopy carbon gain in C_3 and C_4 mono- and dicotyledonoous species. Oecologia 101:504–513

Anten NPR, Schieving F, Medina E, Werger MJA, Schuffelen P (1995b) Optimal leaf area indices in C_3 and C_4 mono- and dicotyledonous species at low and high nitrogen availability. Physiol Plant 95:541–550

Anten NPR, Hikosaka K, Hirose T (2000) Nitrogen utilization and the photosynthetic system. In: Marshal B, Roberts J (eds) Leaf Development and Canopy Growth. Sheffield Academic, Sheffield, pp 171–203

Anten NPR, Hirose T, Onoda Y, Kinugasa T, Kim HY, Okada M, Kobayashi K (2004) Elevated CO_2 and nitrogen availability have interactive effects on canopy carbon gain in rice. New Phytol 161:459–471

Baldocchi D (1994) An analytical solution for coupled leaf photosynthesis and stomatal conductance models. Tree Physiol 14:1069–1079

Baldocchi D (2008) 'Breathing' of the terrestrial biosphere: lessons learned from a global network of carbon dioxide flux measurement systems. Aust J Bot 56:1–26

Baldocchi DD, Harley PC (1995) Scaling carbon dioxide and water vapor exchange from leaf to canopy in a deciduous forest: model testing and application. Plant Cell Environ 18:1157–1173

Baldocchi D, Falge E, Gu L, Olson R, Hollinger D, Running S, Anthoni P, ..., Wofsy S (2001) FLUXNET: a new tool to study the temporal and spatial variability of ecosystem-scale carbon dioxide, water vapor, and energy flux densities. Bull Am Meteorol Soc 82:2415–2434

Ball JT, Woodrow IE, Berry JA (1987) A model predicting stomatal conductance and its contribution to the control of photosynthesis under different environmental conditions. In: Biggins I (ed) Progress in Photosynthesis Research. Martinus Nijhoff, La Hague, pp 221–224

Bonan GB, Lawrence PJ, Oleson KW, Levis S, Jung M, Reichstein M, Lawrence DM, Swenson SC (2011) Improving canopy processes in the Community Land Model version 4 (CLM4) using global flux fields empirically inferred from FLUXNET data. J Geophys Res 116, G02014. doi:10.1029/2010JG001593

Borjigidai A, Hikosaka K, Hirose T (2009) Carbon balance in a monospecific stand of an annual, *Chenopodium album*, at an elevated CO_2 concentration. Plant Ecol 203:33–44

Boysen Jensen P (1932) Die Stoffproduktion der Pflanzen. Gustav Fischer, Jena

Campbell GS, Norman JM (1998) An Introduction to Environmental Biophysics. Springer, New York

Cramer W, Kicklighter DW, Bondeau A, Moore BI, Churkina G, Nemry B, Ruimy A, ..., Potsdam-NPP-model-intercomparison-participants (1999) Comparing global NPP models of terrestrial net primary productivity (NPP): overview and key results. Global Change Biol 5(Suppl 1): 1–15

de Pury DGG, Farquhar GD (1997) Simple scaling of photosynthesis from leaves to canopies without the errors of big-leaf models. Plant Cell Environ 20:537–557

de Wit CT (1965) Photosynthesis of Leaf Canopies. Pudoc, Wageningen

Evers JB (2016) Simulating crop growth and development using functional-structural plant modeling. In: Hikosaka K, Niinemets Ü, Anten N (eds) Canopy Photosynthesis: From Basics to Applications. Springer, Berlin, pp 219–236

Farquhar GD (1989) Models of integrated photosynthesis of cells and leaves. Philos Trans R Soc B 323:357–367

Farquhar GD, von Caemmerer S, Berry JA (1980) A biochemical model of photosynthetic CO_2 assimilation in leaves of C_3 species. Planta 149:78–90

Friend AD (2001) Modeling canopy CO_2 fluxes: are 'big-leaf' simplifications justified? Glob Ecol Biogeogr 10:603–619

Friend AD, Lucht W, Rademacher TT, Keribin RM, Betts R, Cadule P, Ciais P, ..., Woodward FI (2014) Carbon residence time dominates uncertainty in terrestrial vegetation responses to future climate and atmospheric CO_2. Proc Nat Acad Sci USA 111:3280–3285

Garratt JR (1992) The Atmospheric Boundary Layer. Cambridge University Press, Cambridge

Goetz SJ, Prince SD, Goward SN, Thawley MM, Small J (1999) Satellite remote sensing of primary production: an improved production efficiency modeling approach. Ecol Model 122:239–255

Goudriaan J (1977) Crop Micrometeorology: A simulation study, Simulation monographs. Pudoc, Wageningen

Goudriaan J (2016) Light distribution. In: Hikosaka K, Niinemets Ü, Anten N (eds) Canopy Photosynthesis: From Basics to Applications. Springer, Berlin, pp 3–22

Goudriaan J, van Laar HH (1994) Modelling Potential Crop Growth Processes. Kluwer Academic Publishers, Dordrecht

Gu L, Baldocchi DD, Wofsy SC, Munger JW, Michalsky JJ, Urbanski S, Boden TA (2003) Response of a deciduous forest to the Mount Pinatubo eruption: enhanced photosynthesis. Science 299:2035–2038

Gutschick VP (2016) Leaf energy balance: basics, and modeling from leaves to canopies. In: Hikosaka K, Niinemets Ü, Anten N (eds) Canopy Photosynthesis: From Basics to Applications. Springer, Berlin, pp 23–58

Harley PC, Baldocchi DD (1995) Scaling carbon dioxide and water vapour exchange from leaf to canopy in a deciduous forest. I. Leaf model parameterization. Plant Cell Environ 18:1146–1156

Harley PC, Tenhunen JD (1991) Modelling the photosynthetic response of C_3 leaves to environmental factors. In: Boote KJ, Loomis RS (eds) Modelling Crop Photosynthesis – From Biochemistry to Canopy. CSSA, Madison, pp 17–39

Harley PC, Thomas RB, Reynolds JF, Strain BR (1992) Modelling the effects of growth in elevated CO2 on photosynthesis in cotton. Plant Cell Environ 15:271–282

Hikosaka K (2014) Optimal nitrogen distribution within a leaf canopy under direct and diffuse light. Plant Cell Environ 9:2077–2085

Hikosaka K, Shigeno A (2009) The role of Rubisco and cell walls in the interspecific variation in photosynthetic capacity. Oecologia 160:443–451

Hikosaka K, Sudoh S, Hirose T (1999) Light acquisition and use of individuals competing in a dense stand of an annual herb, *Xanthium canadense*. Oecologia 118:388–396

Hikosaka K, Yamano T, Nagashima H, Hirose T (2003) Light-acquisition and use of individuals as influenced by elevated CO_2 in even-aged monospecific stands of *Chenopodium album*. Funct Ecol 17:786–795

Hikosaka K, Noguchi K, Terashima I (2016) Modeling leaf gas exchange. In: Hikosaka K, Niinemets Ü, Anten N (eds) Canopy Photosynthesis: From Basics to Applications. Springer, Berlin, pp 61–100

Hirose T (2005) Development of the Monsi–Saeki theory on canopy structure and function. Ann Bot 95:483–494

Hirose T, Werger MJA (1987a) Nitrogen use efficiency in instantaneous and daily photosynthesis of leaves in the canopy of a *Solidago altissima* stand. Physiol Plant 70:215–222

Hirose T, Werger MJA (1987b) Maximizing daily canopy photosynthesis with respect to the leaf nitrogen allocation pattern in the canopy. Oecologia 72:520–526

Hirose T, Ackerly DD, Traw MB, Ramseier D, Bazzaz FA (1997) CO_2 elevation, canopy photosynthesis, and optimal leaf area index. Ecology 78:2339–2350

Huntzinger DN, Schwalm C, Michalak AM, Schaefer K, King AW, Wei Y, Jacobson A, . . ., Zhu Q (2013) The North American carbon program multi-scale synthesis and terrestrial model intercomparison project: part 1: overview and experimental design. Geosci Model Dev 6:2121–2133

Ichii K, Kondo M, Lee Y-H, Wang S-Q, Kim J, Ueyama M, Lim H-J, . . ., Zaho F-H (2013) Site-level model-data synthesis of terrestrial carbon fluxes in the CarboEastAsia eddy-covariance observation network: toward future modeling efforts. J For Res 18:13–20

Ito A (2011) A historical meta-analysis of global terrestrial net primary productivity: are estimates converging? Glob Chang Biol 17:3161–3175

Ito A, Inatomi M (2012) Water-use efficiency of the terrestrial biosphere: a model analysis on interactions between the global carbon and water cycles. J Hydrometeorol 13:681–694

Ito A, Oikawa T (2002) A simulation model of the carbon cycle in land ecosystems (Sim-CYCLE): a description based on dry-matter production theory and plot-scale validation. Ecol Model 151:147–179

Ito A, Saigusa N, Murayama N, Yamamoto S (2005) Modeling of gross and net carbon dioxide exchange over a cool-temperate deciduous broad-leaved forest in Japan: analysis of seasonal and interannual change. Agric For Meteorol 134:122–134

Kamiyama C, Oikawa S, Kubo T, Hikosaka K (2010) Light interception in species with different functional types coexisting in moorland plant communities. Oecologia 164:591–599

Kramer K, Leinonen KI, Bartelink HH, Berbigier P, Borghetti M, Bernhofer C, Cienciala E, . . ., Vesala T (2002) Evaluation of six process-based forest growth models using eddy-covariance measurements of CO_2 and H_2O fluxes at six forest sites in Europe. Glob Chang Biol 8:213–230

Krinner G, Viovy N, de Noblet-Ducoudré N, Ogée J, Polcher J, Friedlingstein P, Ciais P, . . ., Prentice IC (2005) A dynamic global vegetation model for studies of the coupled atmosphere-biosphere system. Global Biogeochem Cycles 19: GB1015

Kumagai T (2016) Observation and modeling of net ecosystem carbon exchange over canopy. In: Hikosaka K, Niinemets Ü, Anten N (eds) Canopy Photosynthesis: From Basics to Applications. Springer, Berlin, pp 269–287

Kumagai T, Ichie T, Yoshimura M, Yamashita M, Kenzo T, Saitoh TM, Ohashi M, . . ., Komatsu H (2006) Modeling CO_2 exchange over a Bornean tropical rain forest using measured vertical and horizontal variations in leaf-level physiological parameters and leaf area densities. J Geophys Res 111:D10107

Leuning R (1995) A critical appraisal of a combined stomatal-photosynthesis model for C_3 plants. Plant Cell Environ 18:339–355

Levy PE, Cannell MGR, Friend AD (2004) Modelling the impact of future changes in climate, CO_2 concentration and land use on natural ecosystems and the terrestrial carbon sink. Glob Environ Chang 14:21–30

Lieth H (1975) Modeling the primary productivity of the world. In: Lieth H, Whittaker RH (eds) Primary Productivity of the Biosphere. Springer, Berlin, pp 237–263

Lloyd J, Grace J, Miranda AC, Meir P, Miranda HS, Wright IR, Gash JHC, McIntyre J (1995) A simple calibrated model of Amazon rainforest productivity based on leaf biochemical properties. Plant Cell Environ 18:1129–1145

McNaughton KG, Spriggs TW (1986) A mixed layer model for regional evaporation. Bound Lay Meteorol 34:243–262

Melillo JM, McGuire AD, Kicklighter DW, Moore B III, Vörösmarty CJ, Schloss AL (1993) Global climate change and terrestrial net primary production. Nature 363:234–240

Mercado LM, Bellouin N, Sitch S, Boucher O, Huntingford C, Wild M, Cox PM (2009) Impact of

changes in diffuse radiation on the global land carbon sink. Nature 458:1014–1017

Monsi M, Saeki T (1953) Über den Lichtfaktor in den Pflanzengesellschaften und seine Bedeutung für die Stoffproduktion. Jpn J Bot 14:22–52. *Translated as*: Monsi M, Saeki T (2005) On the factor light in plant communities and its importance for matter production. Ann Bot 95:549–567

Monsi M, Uchijima Z, Oikawa T (1973) Structure of foliage canopies and photosynthesis. Annu Rev Ecol Syst 4:301–327

Monteith JL (1972) Solar radiation and productivity of terrestrial ecosystems. J Appl Ecol 9:747–766

Monteith JL (1977) Climate and efficiency of crop production in Britain. Phil Trans R Soc London Ser B 281:277–294

Morales P, Sykes MT, Prentice IC, Smith P, Smith B, Bugmann H, Zierl B, . . ., Ogee J (2005) Comparing and evaluating process-based ecosystem model predictions of carbon and water fluxes in major European forest biomes. Glob Chang Biol 11:2211–2233

Myneni RB, Keeling CD, Tucker CJ, Asrar G, Nemani RR (1997) Increased plant growth in the northern high latitudes from 1981 to 1991. Nature 386:698–702

Nemani RR, Keeling CD, Hashimoto H, Jolly WM, Piper SC, Tucker CJ, Myneni RB, Running SW (2003) Climate-driven increases in global terrestrial net primary production from 1982 to 1999. Science 300:1560–1563

Niinemets Ü (2016) Within-canopy variations in functional leaf traits: structural, chemical and ecological controls and diversity of responses. In: Hikosaka K, Niinemets Ü, Anten N (eds) Canopy Photosynthesis: From Basics to Applications. Springer, Berlin, pp 101–141

Ohtsuka T, Saigusa N, Imura Y, Muraoka H, Koizumi H (2016) Biometric-based estimations of net primary production (NPP) in forest ecosystems. In: Hikosaka K, Niinemets Ü, Anten N (eds) Canopy Photosynthesis: From Basics to Applications. Springer, Berlin, pp 333–351

Papale D, Reichstein M, Aubinet M, Canfora E, Bernhofer C, Kutsch W, Longdoz B, . . ., Yakir D (2006) Towards a standardized processing of net ecosystem exchange measured with eddy covariance technique: algorithms and uncertainty estimation. Biogeosci 3:571–583

Pons TL (2016) Regulation of leaf traits in canopy gradients. In: Hikosaka K, Niinemets Ü, Anten N (eds) Canopy Photosynthesis: From Basics to Applications. Springer, Berlin, pp 143–168

Potter CS, Randerson JT, Field CB, Matson PA, Vitousek PM, Mooney HA, Klooster SA (1993) Terrestrial ecosystem production: a process model based on global satellite and surface data. Global Biogeochem Cycles 7:811–841

Raupach MR (1998) Influences of local feedbacks on land-air exchanges of energy and carbon. Glob Chang Biol 4:477–494

Reichstein M, Falge E, Baldocchi D, Papale D, Aubinet M, Berbigier P, Bernhofer C, . . ., Valentini R (2005) On the separation of net ecosystem exchange into assimilation and ecosystem respiration: review and improved algorithm. Glob Chang Biol 11:1424–1439

Richardson AD, Anderson RS, Arain MA, Barr AG, Bohrer G, Chen G, Chen JM, . . ., Xue Y (2012) Terrestrial biosphere models need better representation of vegetation phenology: results from the North American carbon program site synthesis. Glob Chang Biol 18:566–584

Roderick ML, Farquhar GD, Berry SL, Noble IR (2001) On the direct effect of clouds and atmospheric particles on the productivity and structure of vegetation. Oecologia 129:21–30

Ruimy A, Dedieu G, Saugier B (1996) TURC: a diagnostic model of continental gross primary productivity and net primary productivity. Global Biogeochem Cycles 10:269–285

Running SW, Hunt ERJ (1993) Generalization of a forest ecosystem process model for other biomes, BIOME-BGC, and an application for global-scale models. In: Ehleringer JR, Field CB (eds) Scaling Physiological Processes. Academic Press, San Diego, pp 141–158

Saeki T (1959) Variation of photosynthetic activity with aging of leaves and total photosynthesis in a plant community. Bot Mag Tokyo 72:404–408

Saeki T (1960) Interrelationships between leaf amount, light distribution and total photosynthesis in a plant community. Bot Mag Tokyo 73:55–63

Sasai T, Ichii K, Yamaguchi Y, Nemani R (2005) Simulating terrestrial carbon fluxes using the new biosphere model BEAMS: biosphere model integrating eco-physiological and mechanistic approaches using satellite data. J Geophys Res 110, G02014. doi:10.1029/2005JG000045

Sato H, Ito A, Kohyama T (2007) SEIB–DGVM: a new Dynamic Global Vegetation Model using a spatially explicit individual-based approach. Ecol Model 200:279–307

Schwalm CR, Williams CA, Schaefer K, Anderson R, Arain MA, Baker I, Barr A, . . ., Verma SB (2010) A model-data intercomparison of CO_2 exchange across North America: Results from the North American carbon program site synthesis. J Geophys Res 115:G00H05. doi:10.1029/2009JG001229

Sellers PJ (1985) Canopy reflectance, photosynthesis and transpiration. Int J Remote Sens 6:1335–1372

Sellers PJ, Dickinson RE, Randall DA, Betts AK, Hall FG, Berry JA, Collatz GJ, . . ., Henderson-Sellers A (1997) Modeling the exchanges of energy, water, and carbon between continents and the atmosphere. Science 275:502–509

Sitch S, Smith B, Prentice IC, Arneth A, Bondeau A, Cramer W, Kaplan JO, . . ., Venevsky S (2003) Evaluation of ecosystem dynamics, plant geography and terrestrial carbon cycling in the LPJ dynamic global vegetation model. Glob Chang Biol 9:161–185

Spitters CJT, Schapendonk AHCM (1990) Evaluation of breeding strategies for drought tolerance in potato by means of crop growth simulation. Plant Soil 123:193–203

Tanaka T (1972) Studies on the light-curves of carbon assimilation of rice plants – the interrelation among the light-curves, the plant type and the maximizing yield of rice. Bul Nat Inst Agri Sci A 19:1–100

Terashima I, Saeki T (1985) A new model for leaf photosynthesis incorporating the gradients of light environment and of photosynthetic properties of chloroplasts within a leaf. Ann Bot 56:489–499

Todd-Brown KEO, Randerson JT, Post WM, Hoffman FM, Tarnocai C, Schuur EAG, Allison SD (2013) Causes of variation in soil carbon simulations from CMIP5 Earth system models and comparison with observations. Biogeosciences 10:1717–1736

van Ittersum MK, Lefferlaar PA, van Keulen H, Kropff MJ, Bastiaans L, Goudriaan J (2003) On approaches and applications of the Wageningen crop models. Eur J Agron 18:201–234

Wang YP, Jarvis PG (1990) Description and validation of an array model-MAESTRO. Agr For Meteor 51:257–280

Woodruff DR, McCulloh KA, Meinzer FC (2016) Forest canopy hydraulics. In: Hikosaka K, Niinemets Ü, Anten N (eds) Canopy Photosynthesis: From Basics to Applications. Springer, Berlin, pp 187–217